Interpret Policies in Deep Reinforcement Learning using SILVER with RL-Guided Labeling: A Model-level Approach to High-dimensional and Multi-action Environments

Yiyu Qian[1] **Su Nguyen**[2] **Chao Chen**[3] **Qinyue Zhou**[4] **Liyuan Zhao**[5]
[1]yiyu.qian@student.rmit.edu.au
[2]su.nguyen@rmit.edu.au
[3]chao.chen@rmit.edu.au
[4]qinyuez@umich.edu
[5]liyuanz6@uci.edu

Abstract

Deep reinforcement learning (RL) achieves remarkable performance but lacks interpretability, limiting trust in policy behavior. The existing SILVER framework (Li, Siddique, and Cao 2025) explains RL policy via Shapley-based regression but remains restricted to low-dimensional, binary-action domains. We propose **SILVER with RL-guided labeling**, an enhanced variant that extends SILVER to multi-action and high-dimensional environments by incorporating the RL policy's own action outputs into the boundary points identification. Our method first extracts compact feature representations from image observations, performs SHAP-based feature attribution, and then employs RL-guided labeling to generate behaviorally consistent boundary datasets. Surrogate models, such as decision trees and regression-based functions, are subsequently trained to interpret RL policy's decision structure. We evaluate the proposed framework on two Atari environments using three deep RL algorithms and conduct human-subject study to assess the clarity and trustworthiness of the derived interpretable policy. Results show that our approach maintains competitive task performance while substantially improving transparency and human understanding of agent behavior. This work advances explainable RL by transforming SILVER into a scalable and behavior-aware framework for interpreting deep RL agents in high-dimensional, multi-action settings.

Code — https://github.com/qyy752457002/Interpret-DRL-using-SHAP-Project

Introduction

Deep reinforcement learning (RL) has achieved notable success across diverse domains, including strategic gameplay (e.g., AlphaGo Zero (Shaheen et al. 2025)), Atari games (Jang and Choi 2024), robotics (Tang et al. 2025), and the fine-tuning of large language models (LLMs) (Zhai et al. 2024). These advances are largely attributable to the representational power of deep neural networks (DNNs), which excel at feature extraction and processing high-dimensional data. However, the opaque nature of DNNs poses significant challenges for understanding and interpreting the decision-making processes of RL agents (Murad et al. 2024). This lack of transparency is particularly concerning in high-stakes applications, where interpretability is essential for ensuring safety and trust.

Explainable RL (XRL) has emerged to address similar challenges by enabling human users to understand the decision-making processes of RL agents. Within this context, XRL distinguishes between interpretability and explainability, each with a distinct focus. Interpretability refers to the intrinsic transparency of a model's structure and operation (Li, Siddique, and Cao 2025), often achieved through simpler models such as decision trees (Costa et al. 2024) or logistic regression (Tahirovic and Krivic 2023), which render the policy self-explanatory. Approaches based on this concept are typically categorized as model-level explanation methods (Cheng, Yu, and Xing 2025). Explainability, by contrast, involves post-hoc techniques that provide insights into the behavior of trained models, aiming to clarify or justify their decisions (Li, Siddique, and Cao 2025). These approaches include dataset-level explanation methods, which identify influential data in RL (Cheng, Yu, and Xing 2025). A prominent example is Shapley Additive Explanations (SHAP), which unifies various feature attribution methods within a theoretical framework grounded in Shapley values (Lundberg and Lee 2017). Recent XRL research has applied SHAP to analyze the contribution of individual features in a state to the output of RL value functions (Beechey, Smith, and Şimşek 2023) (Beechey, Smith, and Şimşek 2025). SHAP provides local explanations by assigning numerical importance values to features in specific states (Song et al. 2024), but it does not yield a global understanding of agent behavior.

To bridge the gap between interpretability and explainability, (Li, Siddique, and Cao 2025) introduced the SILVER (Shapley value-based Interpretable policy Via Explanation Regression) framework, which combines SHAP analysis with model-level explanation techniques to interpret deep RL policy. Although effective in relatively simple environments such as CartPole and MountainCar, SILVER relies on two key assumptions: first, that the observation space consists of discrete, well-defined features, which simplifies the computation of Shapley values; and second, that the policy operates within a binary-action setting. Both assumptions fail in complex domains with high-dimensional state

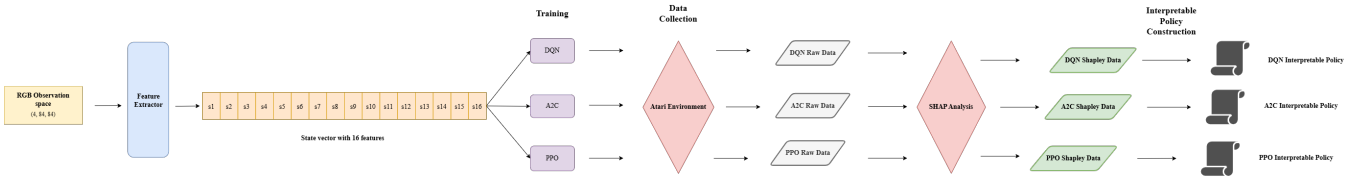

Figure 1: SILVER with RL-Guided Labeling: an overview of the proposed method illustrating the process of feature extraction, deep RL algorithms training, SHAP analysis, and interpretable policy construction

spaces and large action spaces. In such environments, the absence of explicit feature definitions hinders direct SHAP analysis, while the exponential growth of pairwise action boundaries renders binary-action formulations inadequate. Prior XRL studies in high-dimensional domains have attempted to address similar challenges through saliency map visualizations for decision relevance (Samuel Greydanus and Fern 2018) or adapted versions of SHAP in applied contexts such as counter-drone operations (Çetin et al. 2024). Yet, these methods either fail to produce globally interpretable policy or neglect to assess the explanatory effectiveness of their results. Consequently, there remains a pressing need for XRL approaches capable of handling multi-action, high-dimensional environments while providing both interpretability and explainability.

To address these limitations, we propose **SILVER with RL-guided labeling**, an enhanced framework that extends SILVER to multi-action and high-dimensional environments. Our approach integrates the RL policy's own action outputs into the boundary points identification, ensuring that the resulting decision boundaries accurately reflect the agent's actual behavior rather than geometric proximity alone. This modification allows the construction of interpretable policy that remains consistent with RL policy, even in visually complex domains.

This paper makes three primary contributions:

- **Scalable Interpretability in High-Dimensional Environments**: We extend SILVER to operate on visually rich Atari domains, where both the state and action spaces are significantly more complex than in low-dimensional control tasks. This extension enables SHAP analysis on compact feature representations learned from raw RGB observations, enhancing the framework's scalability and robustness.
- **Interpretable Policy Derivation with RL-Guided Labeling**: We introduce a RL-guided labeling mechanism that uses the RL policy's action outputs to annotate boundary points, enabling interpretable policy derivation in multi-action settings. We analyze performance of multiple interpretable models, such as decision trees, linear regression, and logistic regression.
- **Human-Centered Evaluation of Comprehensibility and Trust**: We conduct human-subject study to evaluate how the derived interpretable policy supports user understanding and trust. Through structured feedback, we assess the extent to which these models enhance the perceived transparency and reliability of RL agents' decision-making processes.

Related Work

This section reviews related work on XRL methods in explainability and interpretability.

Explainability

Explainability-focused XRL methods analyze how training data influence policy learning. The influence function (Koh and Liang 2017) estimates the effect of reweighting a sample on model parameters and can be extended to RL for assessing replay transitions.

Shapley values (Shapley 1953) provide a principled foundation for attribution. Extensions such as Data Shapley (Ghorbani and Zou 2019) and FreeShap (Wang et al. 2024) improve scalability and quantify each sample's contribution to policy formation.

Recent studies move beyond static attribution toward behavioral and counterfactual reasoning: process-mining methods (Qian et al. 2025) expose sequential decision logic; SVERL (Beechey, Smith, and Simsek 2025) unifies behavioral and predictive perspectives; and counterfactual explainers (Dong, Zhang, and Feng 2025) illustrate how alternative actions change outcomes.

Interpretability

Interpretability-oriented XRL improves transparency by expressing policies in human-understandable forms (Glanois et al. 2024).

Direct methods design interpretable controllers such as decision trees (Mahbooba et al. 2021) or analytical formulas (Hein, Udluft, and Runkler 2018), with recent advances in differentiable trees via distillation (Gokhale et al. 2024).

Indirect methods first train RL policies and then convert them into interpretable surrogates, e.g., PIRL (Vouros 2022) and VIPER (Saulières 2024).

Our approach follows the indirect paradigm, using Shapley-based RL-guided labeling to transform deep RL policies into compact surrogate models for high-dimensional, multi-action environments, ensuring transparency without sacrificing performance.

Preliminaries

Foundation of Reinforcement Learning

RL is a subfield of machine learning that focuses on training agents to make sequential decisions by interacting with an environment (Sutton and Barto 2018). The environment is framed as a Markov Decision Process (MDP):

- S: The set of possible states of the environment.

- A: The set of available actions for the agent.
- $P(s'|s,a)$: The probability of transitioning from state s to state s' when action a is taken.
- $R(s,a)$: The reward specifies the benefit or cost of executing a particular action a in state s.
- $\gamma \in (0,1)$: The discount factor determines how much a future reward should be discounted compared to a current reward.

The goal of RL is to learn an optimal policy $\pi(a|s)$ that maximizes the agent's long-term reward.

Shapley Values in Reinforcement Learning

The Shapley value (Das 2022) is a concept from cooperative game theory that allocates credit for the total value $v(N)$ earned by a team N among its players. The value is defined as:

$$\phi_i(v) = \sum_{C \subseteq N \setminus \{i\}} \frac{|C|!(n-|C|-1)!}{(n!)} \left[v(C \cup \{i\}) - v(C)\right] \tag{1}$$

where $v(C)$ indicates the value generated by a coalition of players C. The Shapley value $\phi_i(v)$ represents the average marginal contribution of player i when added to all possible coalitions C.

In RL, the state features $\{s_1, ..., s_n\}$ can be treated as players, and the policy output $\pi(s)$ is considered the total value generated by their contributions. To calculate the Shapley values of these features, it is necessary to define a characteristic function $v(C)$ that reflects the model's output for a coalition of features $s_C \subseteq \{s_1, ..., s_n\}$.

Given that the trained policy is undefined for partial inputs s_C, it is important to properly define the characteristic function to ensure accurate Shapley values. Following the on-manifold characteristic value function approach (Frye et al. 2020) (Beechey, Smith, and Şimşek 2023) (Beechey, Smith, and Şimşek 2025), we account for correlations between features rather than assuming their independence.

For a deterministic policy $\pi : S \to A$, which outputs actions, the characteristic function is given by:

$$v^\pi(C) := \pi_C(s) = \sum_{s' \in S} p^\pi(s'|s_C)\pi(s') \tag{2}$$

where $s' = s_C \cup s'_C$, and $p^\pi(s'|s_C)$ is the probability of being in state s' given the partial state features s_C observed under policy π. For a stochastic policy $\pi : S \times A \to [0,1]$, which outputs action probabilities, the characteristic function is:

$$v^\pi(C) := \pi_C(a|s) = \sum_{s' \in S} p^\pi(s'|s_C)\pi(a|s') \tag{3}$$

Methodology

Figure 1 illustrates the pipeline of our methodology. We trained deep RL models using Stable-Baselines3 (Raffin et al. 2021), a widely adopted RL framework, and employed a CNN-based feature extractor to obtain compact representations from raw RGB observations. Using trained deep RL models, we collected data from 1,000 Atari episodes and conducted SHAP analysis on this data to generate Shapley vectors that capture feature contributions to the agent's decision-making. Based on these Shapley vectors, we constructed interpretable policy and subsequently conducted human-subject study to evaluate the comprehensibility and trustworthiness of the derived policy.

Feature Extraction

Figure 9 shows our CNN-based feature extractor, which converts stacked RGB Atari frames $(4, 84, 84)$ into a compact state vector of 16 features. Such low-dimensional representations are critical for achieving stable and efficient policy learning, as they distill high-dimensional visual inputs into task-relevant features while minimizing redundancy (Echchahed and Castro 2025). This design is fully compatible with Stable-Baselines3, using the NatureCNN encoder within the CnnPolicy architecture.

SHAP Analysis

Following the SILVER framework, we compute each feature's attribution $\phi_i(v^\pi)$—the marginal contribution of feature i in state s under policy π. Specifically, we plug Eq. (2) or Eq. (3) into the Shapley definition in Eq. (1).

These attributions indicate how features steer the policy's choice. For example, in a two-action setting ($a_1 = -1$, $a_2 = 1$), a positive $\phi_i(v^\pi)$ suggests feature i pushes the policy toward a_2, while a negative value pulls it toward a_1. Because features with identical marginal effects receive the same score, symmetries in policy reasoning are directly revealed. Finally, we collect all feature attributions into the vector

$$\Phi_s = (\phi_1, \ldots, \phi_n),$$

and cluster these vectors to identify groups of states that induce similar action preferences, thereby further gives insights into action-group boundaries.

Interpretable Policy Construction

This section describes how we construct interpretable policy. The complete algorithm is presented in Algorithm 1. It consists of four stages:

- **Action K-Means Clustering**: Group Shapley vectors into $|A|$ clusters corresponding to the agent's discrete actions.
- **Boundary Points Identification**: Locate boundary points between action clusters.
- **Inverse Mapping and RL-Guided Labeling**: Map boundary points back to their corresponding states and query the RL policy to assign action labels to each state.
- **Interpretable Models Fitting**: Fit decision trees, linear regression, and logistic regression to approximate decision boundaries.

Action K-Means Clustering For each state s, we compute its Shapley vector $\Phi_s \in \mathbb{R}^n$, where each entry quantifies the marginal contribution of a feature. We then perform K-means clustering with $k = |A|$ clusters, equal to the number of discrete actions:

$$\arg\min_{A} \sum_{i=1}^{k} \sum_{\Phi_s \in A_i} \|\Phi_s - \mu_i\|^2, \tag{4}$$

where μ_i is the centroid of cluster A_i:

$$\mu_i = \frac{1}{|A_i|} \sum_{\Phi_s \in A_i} \Phi_s.$$

This ensures that each action is associated with a representative cluster of Shapley vectors.

Boundary Points Identification After forming clusters, boundaries between different action regions can be identified through the use of boundary points. A *boundary point* X lies at the interface of two clusters A_i and A_j, where the policy exhibits equal likelihood of choosing either action. This condition reflects uncertainty in the policy's action selection at a given state, and thus X represents a critical decision boundary. Formally, the boundary point is determined by minimizing the difference between its distances to the two cluster centroids:

$$\arg\min_{X} \left(\|X - \mu_i\|^2 - \|X - \mu_j\|^2 \right), \tag{5}$$

where μ_i and μ_j denote the centroids of points in A_i and A_j, respectively.

Inverse Mapping and RL-Guided Labeling Once boundary points are identified in the Shapley vector space, they must be mapped back to their corresponding states in the original environment. We follow the *Inverse Shapley Mapping* defined by (Li, Siddique, and Cao 2025):

$$\phi_i^{-1} : \phi_i(v) \rightarrow \{i\},$$

which recovers the original state s associated with a given Shapley vector Φ_s.

The original SILVER framework was designed for binary-action environments. It assumes that states with similar Shapley vectors correspond to the same action, allowing decision boundaries to be inferred purely from distances between action clusters in the Shapley vector space. This assumption holds in binary-action settings ($a_1 = left$ and $a_2 = right$), where each boundary point naturally lies between two well-defined action clusters. In multi-action environments, however, this geometric assumption breaks down. A single state may lie near several action clusters in the Shapley vector space, making it unclear which action the boundary point truly represents. As the number of actions increases, the number of possible action pairs grows rapidly, and distances in Shapley vector space no longer provide reliable information about RL agent's actual decision-making behavior. Consequently, boundary points defined solely by geometric proximity become ambiguous and cannot be used to train accurate interpretable models.

To resolve this problem, we introduce a *RL-guided labeling mechanism*. Table 1 shows the comparison between SILVER and SILVER with RL-guided labeling.

After reconstructing each boundary state s_{ij} through inverse mapping, we query the trained RL policy π to obtain the corresponding action:

$$a_{ij} = \pi(s_{ij}).$$

This step ensures that every boundary point receives an action label derived directly from the RL policy. By combining inverse mapping with RL-guided labeling, we obtain a behaviorally consistent boundary dataset (s_{ij}, a_{ij}), which enables reliable training of interpretable models that approximate decision boundaries.

Interpretable Models Fitting For labeled boundary states $\{(s_{ij}, a_{ij})\}$, we fit interpretable models. Unlike (Li, Siddique, and Cao 2025), which employed linear regression exclusively, we explore multiple interpretable models to capture different aspects of policy behavior. Specifically, decision tree exposes hierarchical if–then reasoning patterns, linear regression yields direct coefficient-based explanations, and logistic regression represents softmax probabilities among actions.

Human Study

To assess the interpretability and trustworthiness of our framework, we conducted a human-subject study, following recent XRL evaluation standards (Kohler et al. 2025) (Alabdulkarim et al. 2025). The study consists of two tasks designed to measure participants' ability to comprehend and trust interpretable policy.

Policy Comprehension Task Participants are presented with selected states from Atari environments, together with the corresponding interpretable policy. They are asked to manually infer which action the agent would take based on interpretable policy, following the policy interpretability protocol proposed by (Kohler et al. 2025). This task evaluates how effectively humans can understand and predict the agent's actions based on interpretable policy.

Trust Calibration Task Participants are presented with paired gameplay clips of agents acting under either the original policy or a fixed interpretable policy. They are asked to rate how much they trust each agent's decisions using a 5-point Likert scale, adapted from the interpretability evaluation survey implemented in (Sarch et al. 2025). This task assesses how reliably and consistently humans perceive the surrogate policy compared to the original policy.

Experiments

To evaluate the effectiveness of SILVER with RL-guided labeling, we performed experiments. To assess scalability, we applied our framework to high-dimensional RGB environments from the Atari benchmark, which presents substantially more complex state and action spaces than classical control tasks. To derive interpretable policy, we employed

classification-based and regression-based techniques, including decision trees, linear regression, and logistic regression, thereby enabling an examination of the trade-offs between model interpretability and policy performance. To test real-world applicability, we conducted human-subject study to evaluate the comprehensibility and trustworthiness of the derived policy.

All Atari environments were wrapped using the `Atari Wrappers` from Stable-Baselines3, which clip rewards to $[-1, 0, 1]$ by its sign for training stability.

The experimental results demonstrate that SILVER with RL-guided labeling scales effectively to complex environments, produces interpretable policy that balances transparency with performance, and enhances user trust and confidence in the decision-making of RL agents.

MsPacman

The MsPacman environment is a maze-based Atari game where the agent navigates to collect rewards and avoid ghosts. The observation space consists of high-dimensional RGB frames showing MsPacman, pellets, fruits, and ghosts. The action space includes 9 discrete movements with or without the fire button. The agent gains rewards for consuming pellets and fruits, and receives a penalty when caught by a ghost. The goal is to maximize the cumulative score through strategic navigation.

We sampled state distributions from 1000 episodes collected by each deep RL algorithm. For every sampled state, we computed the Shapley values of its features using Equation (5), thereby obtaining a Shapley vector that quantifies the contribution of individual features to the policy's decision. Figures 2 presents the Shapley values of 16 features for DQN, PPO, and A2C, respectively.

Based on these Shapley values, we applied k-means clustering to the action space in order to identify cluster centroids, with each cluster corresponding to a distinct action region. Since MsPacman comprises 9 discrete actions, we formed 9 clusters and computed boundary points between them, yielding 36 boundary points in total.

Subsequently, we reconstructed boundary points in the original state space by inverting Shapley values. Tables 2, 3, 4, 5, 6, 7 report the boundary points and their Shapley-inverse counterparts for each algorithm. Finally, we applied decision trees, linear regression, and logistic regression to obtain interpretable policy for DQN, PPO, and A2C.

Decision Tree Figures 10, 11, and 12 illustrate decision trees for PPO, A2C, and DQN, respectively.

Taking PPO as an example, consider the first row in Table 7. Starting from the root node of Figure 10, the decision process proceeds as follows:

1. At the root node, check $Feature_{12} \leq 14173.283$.
   Since $8493.874 < 14173.283$, move to the **left child**.
2. Next, check $Feature_4 \leq 2304.729$.
   Since $530.9578 < 2304.729$, move to the **left child**.
3. Then, check $Feature_2 \leq 6694.608$.
   Since $5753.206 < 6694.608$, move to the **left child** and reach a leaf: $\boxed{\text{class} = 7}$, which corresponds to $\boxed{\text{action} = 7}$.

Linear Regression Table 14 illustrates the interpretable policy boundaries derived from linear regression for PPO, A2C, and DQN. Here, x_1 through x_{16} represent the 16 state features used in the analysis.

Taking PPO as an example, consider the second row in table 7. Substituting the feature values into the decision boundary in table 14, we obtain:

$$\begin{aligned} f(x) = 7.37 \\ &+ (2.77 \times 10^{-4}) \times 6628.804 \\ &- (1.94 \times 10^{-4}) \times 1914.645 \\ &- (5.66 \times 10^{-4}) \times 1880.883 \\ &+ (1.29 \times 10^{-5}) \times 14349.77 \\ &- (1.35 \times 10^{-4}) \times 11766.16 \\ &\approx 6.37. \end{aligned}$$

Taking the floor of this value yields $\boxed{f(x) = 6}$, which corresponds to $\boxed{\text{action} = 6}$.

Although actions are discrete, linear regression serves as a continuous decision boundary function. Its outputs are discretized (via flooring) to recover action indices, yielding a concise and interpretable mapping from state features to actions.

Logistic Regression Table 17, Table 16, and Table 18 illustrate the interpretable policy boundaries derived from logistic regression for A2C, PPO, and DQN.

Taking PPO as an example, consider the third row in Table 7. Substituting the feature values into the corresponding decision boundaries in Table 16, we obtain the following logits:

$$\begin{aligned} f_5(x) \approx -8.93, \quad f_6(x) \approx 26.12, \\ f_7(x) \approx -33.03, \quad f_8(x) \approx 16.12. \end{aligned}$$

Applying the softmax function to these logits converts them into normalized probabilities:

$$P(a = i \mid x) = \frac{e^{f_i(x)}}{\sum_j e^{f_j(x)}}.$$

The predicted action is then determined by selecting the one with the highest probability:

$$\hat{a} = \arg\max_i P(a = i \mid x).$$

For this state, the highest probability corresponds to $\boxed{f_6(x)}$, indicating that the model predicts $\boxed{\text{action} = 6}$.

RoadRunner

We also evaluated our framework on RoadRunner. Details of the experiment are provided in Appendix D.

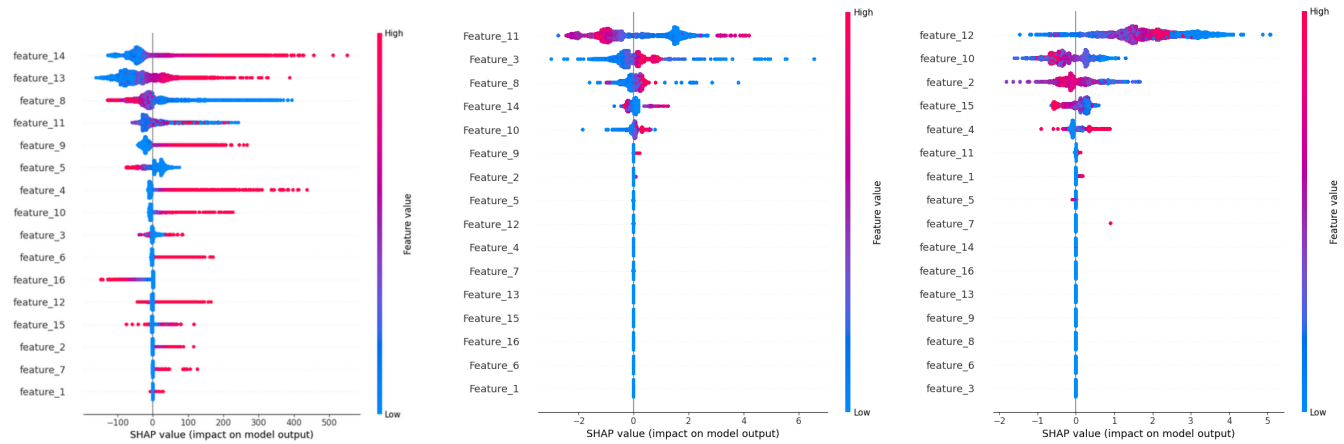

(a) MsPacman DQN - SHAP value (b) MsPacman A2C - SHAP value (c) MsPacman PPO - SHAP value

Figure 2: SHAP value comparison of MsPacman under different algorithms (DQN, A2C, PPO)

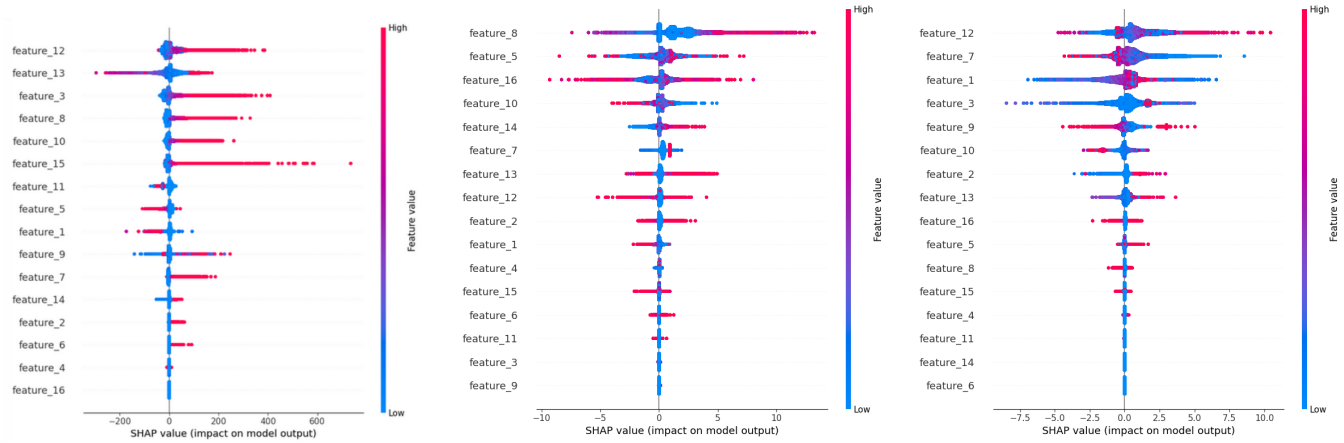

(a) RoadRunner DQN - SHAP value (b) RoadRunner A2C - SHAP value (c) RoadRunner PPO - SHAP value

Figure 3: SHAP value comparison of RoadRunner under different algorithms (DQN, A2C, PPO)

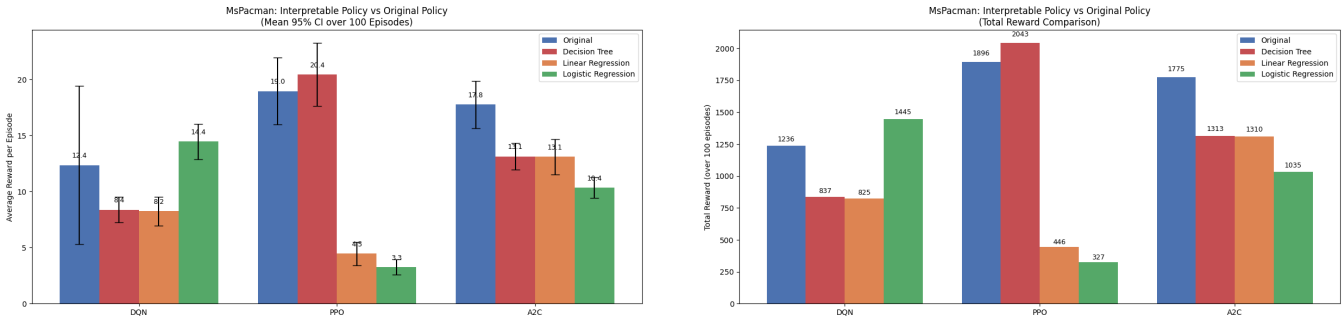

(a) MsPacman: interpretable policy vs original policy (mean 95% CI over 100 episodes)

(b) MsPacman: interpretable policy vs original policy (total reward comparison)

Figure 4: Performance comparison between interpretable and original policies in MsPacman

Fidelity Score

Fidelity measures how well the surrogate policy covers the original policy (Altmann et al. 2025). The fidelity function proposed by (Li, Siddique, and Cao 2025) further quantifies the behavioral difference between the interpretable policy and the original policy:

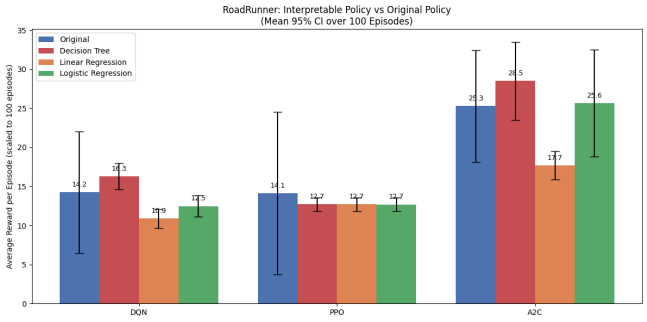

(a) RoadRunner: interpretable policy vs original policy (mean 95% CI over 100 episodes)

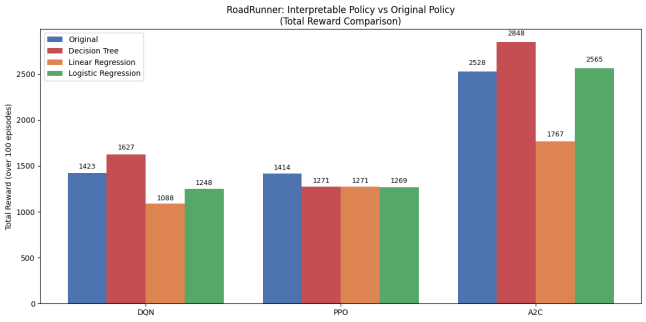

(b) RoadRunner: interpretable policy vs original policy (total reward comparison)

Figure 5: Performance comparison between interpretable and original policies in RoadRunner

$$F(\pi_{\text{interp}}, \pi_{\text{orig}}) = \frac{1}{|S|} \sum_{s \in S} \mathbb{1}\{\pi_{\text{interp}}(s) = \pi_{\text{orig}}(s)\}, \quad (6)$$

where the original policy is treated as the ground truth.

Building on this notion, we define our fidelity score explicitly as the percentage of states where the interpretable and original policies output the same action.

Figure 6 shows the fidelity scores across all environments and algorithms.

Human Study

We conducted a human-subject study with 30 participants who had prior training in RL. To simplify evaluation and minimize cognitive burden, the study was restricted to the MsPacman environment and sole interpretable model. Since decision tree outperformed the PPO policy and provided the clearest if–then style rules, we selected it for evaluation.

Design Participants were presented with representative MsPacman states, together with the decision tree. Their task was to infer the action chosen by the decision tree. While doing so, we collected their action inferences, response times, and subjective trust ratings.

Metrics We measured three aspects:

- **Response Time**: The average time taken to make an action inference, reflecting the efficiency of interpretability.
- **Accuracy**: The proportion of participant-inferred actions that matched the actual decision-tree outputs, reflecting the correctness of human interpretation.
- **Trust Ratings**: After completing all 4 trials, participants rated their overall trust in the decision-tree surrogate on a 5-point Likert scale, where:
  - 1 = Very Low Trust (I would not rely on this model's decisions at all)
  - 2 = Low Trust (I have limited confidence; decisions often appear unreliable)
  - 3 = Neutral (I am undecided; the model's decisions sometimes make sense, sometimes not)
  - 4 = High Trust (I generally have confidence in the model's decisions, though not absolute)
  - 5 = Very High Trust (I would fully rely on this model's decisions with strong confidence)

Discussion

MsPacman Decision tree derived from PPO slightly outperformed the original policy, whereas linear regression and logistic regression performed noticeably worse. For DQN and A2C, surrogate models were marginally below their RL baselines. Decision trees generally achieved the best and linear regression the weakest performance. An exception appeared in DQN, where logistic regression surpassed the decision tree. SHAP analyses revealed that high-index features (> 10) contributed most to policy outputs: feature 12 in PPO, features 13, 14 in DQN, and feature 11 in A2C.

RoadRunner Decision trees from DQN and A2C slightly outperformed the original algorithms, while logistic regression under A2C achieved comparable results. Overall, decision trees remained strongest and linear regression weakest, except in PPO where all interpretable models performed similarly but below the original. Unlike MsPacman, features with lower indices also had strong influence, such as feature 8 in A2C and feature 3 in DQN.

Fidelity Score A high fidelity score does not necessarily imply strong task performance. For example, PPO's logistic regression in MsPacman had high fidelity (82.9%) but low performance, whereas the DQN decision tree in RoadRunner achieved superior performance despite low fidelity (54.7%). Hence, fidelity reflects alignment between surrogate and RL policies but not their task-level effectiveness.

Limitation

Our work has three limitations that may need to be addressed in the future work:

Loss of Semantic Meaning in Feature Extraction The extracted state features lack explicit semantic meanings. Unlike classic control environments (e.g., CartPole, MountainCar) with well-defined variables, our state vectors lack

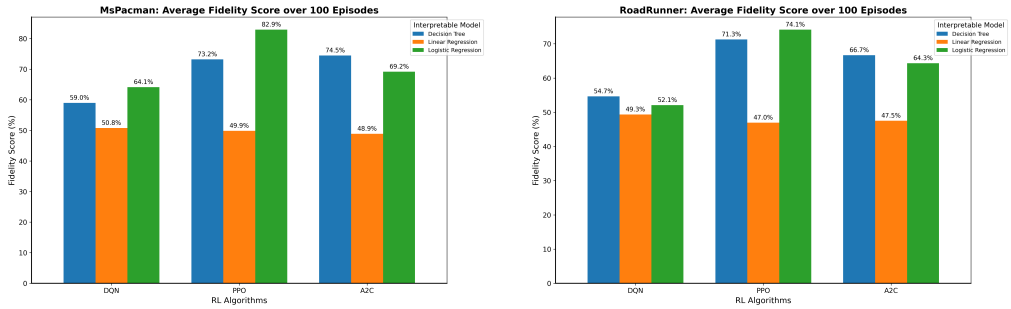

(a) MsPacman: average fidelity score over 100 episodes

(b) RoadRunner: average fidelity score over 100 episodes

Figure 6: Average fidelity scores of interpretable policies across MsPacman and RoadRunner

such semantic clarity. We plan to integrate Vision Language Models (VLMs) (Chen et al. 2024) to derive semantically grounded state features from complex, high-dimensional observations.

Limited to Atari Environments Although the framework has been evaluated in complex Atari domains, these environments do not fully represent real-world decision-making scenarios. With the growing interest in explainable RL fine-tuning for LLMs, extending the framework to transformer-based deep RL algorithms (e.g., GRPO, DAPO, GSPO) represents a promising future direction. In such contexts, user prompts could be modeled as observations, while the LLM's output tokens serve as actions.

Restricted Scope of Human-subject Study The human-subject experiment was conducted on a single environment with one interpretable policy. Future work could involve broader evaluations across multiple environments and diverse interpretable policy forms to better assess generalizability and human comprehension.

Conclusion

In this paper, we propose SILVER with RL-guided labeling, a framework designed to generate interpretable policies for deep RL algorithms. Experimental results demonstrate that our method achieves performance comparable to deep RL algorithms in high-dimensional and multi-action environments, while preserving human comprehensibility and trust.

Potential future work includes: (1) refining the feature extraction process to assign semantic meaning to each state feature, (2) extending the framework to LLMs environments, particularly in the context of RL fine-tuning, and (3) conducting human-subject studies with diverse interpretable models to systematically compare their performance on comprehension and trust.

Acknowledgments

We sincerely thank all volunteers who participated in our human-subject study. We are also grateful to our colleagues at the RMIT University Data Analytics Hub for their continuous encouragement and support. We further acknowledge Bingchen Lu, model engineer at Fannie Mae and our undergraduate colleague from the University of California, Irvine, for his assistance in designing the human-subject study. Special thanks are extended to Dr. Ting Dang, Senior Lecturer at the University of Melbourne, for her insightful feedback and valuable guidance during the paper revision process.

References

Alabdulkarim, A.; Singh, M.; Mansi, G.; Hall, K.; Ehsan, U.; and Riedl, M. O. 2025. Experiential explanations for reinforcement learning. *Neural Computing and Applications*, 1–31.

Altmann, P.; Davignon, C.; Zorn, M.; Ritz, F.; Linnhoff-Popien, C.; and Gabor, T. 2025. Surrogate Fitness Metrics for Interpretable Reinforcement Learning. *arXiv preprint arXiv:2504.14645*.

Beechey, D.; Smith, T.; and Şimşek, Ö. 2025. A Theoretical Framework for Explaining Reinforcement Learning with Shapley Values. *arXiv preprint arXiv:2505.07797*.

Beechey, D.; Smith, T. M.; and Şimşek, Ö. 2023. Explaining reinforcement learning with shapley values. In *International Conference on Machine Learning*, 2003–2014. PMLR.

Beechey, T.; Smith, A.; and Şimşek, O. 2025. SVERL: A Theoretical Framework for Explaining Reinforcement Learning with Shapley Values. *arXiv preprint arXiv:2505.07797*.

Çetin, E.; Barrado, C.; Salamí, E.; and Pastor, E. 2024. Analyzing deep reinforcement learning model decisions with Shapley additive explanations for counter drone operations. *Applied Intelligence*, 54(23): 12095–12111.

Chen, W.; Mees, O.; Kumar, A.; and Levine, S. 2024. Vision-language models provide promptable representations for reinforcement learning. *arXiv preprint arXiv:2402.02651*.

Cheng, Z.; Yu, J.; and Xing, X. 2025. A Survey on Explainable Deep Reinforcement Learning. *arXiv preprint arXiv:2502.06869*.

Costa, V. G.; Pérez-Aracil, J.; Salcedo-Sanz, S.; and Pedreira, C. E. 2024. Evolving interpretable decision trees for reinforcement learning. *Artificial Intelligence*, 327: 104057.

Das, D. 2022. Values of N-Person Games with Indivisibility and Complementarity. *Available at SSRN 4073731*.

Dong, Y.; Zhang, R.; and Feng, W. 2025. Counterfactual Explanations for Continuous-Action Reinforcement Learning. *arXiv preprint arXiv:2505.12701*.

Echchahed, A.; and Castro, P. S. 2025. A Survey of State Representation Learning for Deep Reinforcement Learning. *arXiv preprint arXiv:2506.17518*.

Frye, C.; de Mijolla, D.; Begley, T.; Cowton, L.; Stanley, M.; and Feige, I. 2020. Shapley explainability on the data manifold. *arXiv preprint arXiv:2006.01272*.

Ghorbani, A.; and Zou, J. 2019. Data Shapley: Equitable Valuation of Data for Machine Learning. *Proceedings of ICML*.

Glanois, C.; Weng, P.; Zimmer, M.; Li, D.; Yang, T.; Hao, J.; and Liu, W. 2024. A survey on interpretable reinforcement learning. *Machine Learning*, 1–44.

Gokhale, G.; Karimi Madahi, S. S.; Claessens, B.; and Develder, C. 2024. Distill2Explain: Differentiable decision trees for explainable reinforcement learning in energy application controllers. In *Proceedings of the 15th ACM International Conference on Future and Sustainable Energy Systems*, 55–64.

Hein, D.; Udluft, S.; and Runkler, T. A. 2018. Interpretable policies for reinforcement learning by genetic programming. *Engineering Applications of Artificial Intelligence*, 76: 158–169.

Jang, S.; and Choi, C. 2024. Analyzing State Space Similarities for Multi-Task Deep Reinforcement Learning in Atari Games. In *2024 15th International Conference on Information and Communication Technology Convergence (ICTC)*, 1501–1502. IEEE.

Koh, P. W.; and Liang, P. 2017. Understanding black-box predictions via influence functions. *Proc. of ICML*.

Kohler, H.; Delfosse, Q.; Radji, W.; Akrour, R.; and Preux, P. 2025. Evaluating Interpretable Reinforcement Learning by Distilling Policies into Programs. *arXiv preprint arXiv:2503.08322*.

Li, P.; Siddique, U.; and Cao, Y. 2025. From Explainability to Interpretability: Interpretable Policies in Reinforcement Learning Via Model Explanation. *arXiv preprint arXiv:2501.09858*.

Lundberg, S. M.; and Lee, S.-I. 2017. A unified approach to interpreting model predictions. *Advances in neural information processing systems*, 30.

Mahbooba, B.; Timilsina, M.; Sahal, R.; and Serrano, M. 2021. Explainable artificial intelligence (XAI) to enhance trust management in intrusion detection systems using decision tree model. *Complexity*, 2021(1): 6634811.

Murad, N. Y.; Hasan, M. H.; Azam, M. H.; Yousuf, N.; and Yalli, J. S. 2024. Unraveling the black box: A review of explainable deep learning healthcare techniques. *IEEE Access*.

Qian, Y.; Miller, T.; Qian, Z.; and Zhao, L. 2025. Exploring Explainable Multi-player MCTS-minimax Hybrids in Board Game Using Process Mining. *arXiv preprint arXiv:2503.23326*.

Raffin, A.; Hill, A.; Gleave, A.; Kanervisto, A.; Ernestus, M.; and Dormann, N. 2021. Stable-baselines3: Reliable reinforcement learning implementations. *Journal of machine learning research*, 22(268): 1–8.

Samuel Greydanus, J. D., Anurag Koul; and Fern, A. 2018. Visualizing and understanding atari agents. In *Proc. of ICML*.

Sarch, G.; Saha, S.; Khandelwal, N.; Jain, A.; Tarr, M. J.; Kumar, A.; and Fragkiadaki, K. 2025. Grounded Reinforcement Learning for Visual Reasoning. *arXiv preprint arXiv:2505.23678*.

Saulières, L. 2024. *Explaining reinforcement learning*. Ph.D. thesis, Université de Toulouse.

Shaheen, A.; Badr, A.; Abohendy, A.; Alsaadawy, H.; and Alsayad, N. 2025. Reinforcement learning in strategy-based and atari games: A review of google deepminds innovations. *arXiv preprint arXiv:2502.10303*.

Shapley, L. S. 1953. *A Value for n-Person Games*, volume 2.

Song, X.; HSIEH, W.-C.; Bi, Z.; Jiang, C.; Liu, J.; Peng, B.; Zhang, S.; Pan, X.; Xu, J.; Wang, J.; et al. 2024. A Comprehensive Guide to Explainable AI: From Classical Models to LLMs.

Sutton, R. S.; and Barto, A. G. 2018. *Reinforcement Learning: An Introduction*. The MIT Press, 2nd edition.

Tahirovic, E.; and Krivic, S. 2023. Interpretability and Explainability of Logistic Regression Model for Breast Cancer Detection. In *ICAART (3)*, 161–168.

Tang, C.; Abbatematteo, B.; Hu, J.; Chandra, R.; Martín-Martín, R.; and Stone, P. 2025. Deep reinforcement learning for robotics: A survey of real-world successes. In *Proceedings of the AAAI Conference on Artificial Intelligence*, volume 39, 28694–28698.

Vouros, G. A. 2022. Explainable deep reinforcement learning: state of the art and challenges. *ACM Computing Surveys*, 55(5): 1–39.

Wang, J.; Lin, X.; Qiao, R.; Foo, C.-S.; and Low, B. K. H. 2024. Helpful or Harmful Data? Fine-tuning-Free Shapley Attribution for Explaining Language Model Predictions. *Proceedings of ICML*.

Zhai, S.; Bai, H.; Lin, Z.; Pan, J.; Tong, P.; Zhou, Y.; Suhr, A.; Xie, S.; LeCun, Y.; Ma, Y.; et al. 2024. Fine-tuning large vision-language models as decision-making agents via reinforcement learning. *Advances in neural information processing systems*, 37: 110935–110971.

Appendix A: SILVER with RL-Guided Labeling

Algorithm 1: SILVER with RL-Guided Labeling

Input: Shapley vectors $(\Phi_{s_1}, \Phi_{s_2}, \ldots, \Phi_{s_m})$, corresponding states $(s_1, s_2, \ldots, s_m)$, trained RL policy π

Parameter: Number of discrete actions k

Output: Interpretable decision boundary functions $\{f_{ij}\}$ for each pair of actions (i, j)

Step 1: Action Clustering

$A = \{A_1, \ldots, A_k\} \leftarrow$ K-Means$(\{\Phi_{s_i}\}_{i=1}^{m}, k)$

for $i = 1$ **to** k **do**

  $\mu_i \leftarrow \frac{1}{|A_i|} \sum_{\Phi \in A_i} \Phi$ `// Compute cluster centroids`

Step 2: Boundary Points Identification

Initialize empty set of boundary points $B \leftarrow \{\}$

for $i = 1$ **to** $k - 1$ **do**

  for $j = i + 1$ **to** k **do**

    $X_{ij} \leftarrow \arg\min_{X \in \{\Phi_s\}} \left| \|X - \mu_i\|^2 - \|X - \mu_j\|^2 \right|$ `// Find geometric boundary point`

    $s_{ij} \leftarrow \phi^{-1}(X_{ij})$ `// Inverse mapping to state space`

    $a_{ij} \leftarrow \pi(s_{ij})$ `// Query RL policy for action label`

    $B \leftarrow B \cup \{(s_{ij}, a_{ij})\}$ `// Store labeled boundary point`

Step 3: Interpretable Models Fitting

$f_{ij}(s) \leftarrow$ Fit Interpretable Model(B)

Step 4: Output

return $\{f_{ij}\}$ *as pairwise decision boundary functions*

Appendix B: Comparison between SILVER and SILVER with RL-Guided Labeling

Aspect	SILVER (Li, Siddique, and Cao 2025)	SILVER with RL-Guided Labeling
Target environments	Restricted to binary-action, low-dimensional tasks (e.g., CartPole, MountainCar)	Scalable to high-dimensional, multi-action environments (up to 18 discrete actions)
Boundary identification	Determined purely by geometric distances between action clusters in Shapley vectors	Retains geometric identification but assigns action labels to each boundary state based on the output of RL policy $\pi(s_{ij})$
Labeling mechanism	Implicitly determined by nearest cluster pairs in Shapley vectors	Explicitly determined by querying the RL policy for action labels
Resulting data	Boundary samples may be ambiguous or misaligned with the actual RL policy behavior	Behaviorally consistent dataset (s_{ij}, a_{ij}) enabling reliable interpretable models training

Table 1: Comparison between SILVER and SILVER with RL-Guided Labeling

Appendix C: Gameplay Clips and Feature Extractor

Figure 7: Gameplay clips of PPO in MsPacmanNoFrameskip-v4

Figure 8: Gameplay clips of PPO in RoadRunnerNoFrameskip-v4

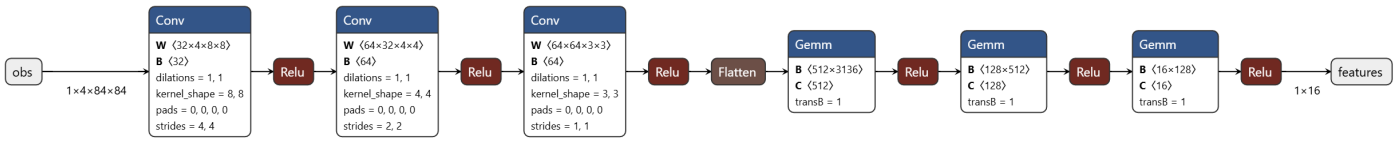

Figure 9: CNN-based feature extractor

Appendix D: Experiment on RoadRunner

The RoadRunner environment is a fast-paced Atari game where the agent controls the roadrunner to evade the pursuing coyote across desert terrain. The observation space consists of high-dimensional RGB frames depicting the roadrunner, the coyote, bird seed, and obstacles. The action space includes 18 discrete controls for movement, jumping, ducking, and firing. The agent gains rewards for collecting bird seed and avoiding capture, and penalties for collisions or being caught. The objective is to maximize survival while efficiently collecting rewards.

The contributions of state features to RL policy's decisions are visualized in Figure 3. Based on these Shapley representations, we applied k-means clustering to the 18-action space and identified 153 boundary points that separate distinct behavioral regions.

Tables 8, 9, 11, 10, 11, 12, 13 report the boundary points and their Shapley-inverse counterparts for each deep RL algorithm.

Decision Tree Figure 13, 14, and 15 present decision trees for PPO, A2C, and DQN, respectively.

Taking A2C as an example, consider the first row in Table 11. Starting from the root node of Figure 14, the decision process unfolds as follows:

1. At the root node, check whether $Feature_8 \leq 399.381$. Since $1037.385 > 399.381$, the process moves to the **right child**.
2. Next, check whether $Feature_{11} \leq 0.342$. Since $0 < 0.342$, the process moves to the **left child**.
3. Then, check whether $Feature_7 \leq 148.991$. Since $0 < 148.991$, the process moves to the **left child**.
4. Finally, check whether $Feature_8 \leq 466.391$. Since $1037.385 > 466.391$, the process moves to the **right child**, reach a leaf: $\boxed{\text{class} = 7}$, which corresponds to $\boxed{\text{action} = 7}$.

Linear Regression Table 15 illustrates the interpretable policy boundaries derived from linear regression for PPO, A2C, and DQN. Here, x_1 through x_{16} represent the 16 state features used in the analysis.

Taking A2C as an example, consider the second row in Table 11. Substituting the feature values into the decision boundary in Table 15, we obtain:

$$\begin{aligned} f(x) = 8.82 \\ &- (9.00 \times 10^{-4}) \times 95.19944 \\ &- (6.94 \times 10^{-4}) \times 470.2562 \\ &- (1.03 \times 10^{-3}) \times 180.0636 \\ &- (4.19 \times 10^{-4}) \times 88.72929 \\ &+ (1.34 \times 10^{-3}) \times 96.3101 \\ &+ (1.08 \times 10^{-3}) \times 647.2335 \\ &\approx 9.01. \end{aligned}$$

Taking the floor of this value yields $\boxed{f(x) = 9}$, which corresponds to $\boxed{\text{action} = 9}$.

Logistic Regression Table 20 illustrates the interpretable policy boundaries derived from logistic regression for A2C. Taking the third row of features in Table 11, we substitute the values into the corresponding decision boundaries. This yields a set of logits $\{f_2(x), f_4(x), f_5(x), f_7(x), f_9(x)\}$, each associated with one action. The procedure is identical to that already demonstrated for the MsPacman environment.

Appendix E: Boundary Points and SHAP Inverse Boundary Points

Feature 1	Feature 2	Feature 3	Feature 4	Feature 5	Feature 6	Feature 7	Feature 8
0.053718	-0.58133	-1.57969	-10.0231	10.97137	-3.29043	-0.34815	-0.07359
-0.13582	0.166289	17.79752	-8.14196	16.23918	0.061392	0.271136	362.5037
-0.06903	-0.93946	21.95477	194.3563	54.4827	-3.42446	-0.39898	104.8359
0.147134	-0.61962	21.12769	11.61575	41.8084	-5.48569	-0.59579	61.4086
-0.08426	-0.2127	-3.38793	-5.58269	-26.1117	-0.91717	-0.01381	-45.8628
-0.09114	-0.1284	18.9745	-8.89167	29.9608	-2.01041	-0.14159	269.8545
0.108812	-0.73049	6.476514	-10.0114	31.2885	-3.58155	-0.38707	-6.30191
0.250599	-1.08509	16.77061	79.48419	36.1719	-5.36885	-0.59214	69.85063
-0.10688	-0.31807	14.7685	-10.9438	26.3507	-3.13208	-0.13384	222.8886
-0.03265	-0.36164	1.063268	-10.739	17.4609	-2.72974	-0.17212	68.40194

Feature 9	Feature 10	Feature 11	Feature 12	Feature 13	Feature 14	Feature 15	Feature 16	Action Label
-28.4395	-9.43087	-0.56828	0.880025	93.17239	-66.1944	-1.10136	1.182046	6
-28.2911	-8.78055	-28.6062	79.80954	-71.0975	-74.9427	-5.54564	1.781113	2
131.3282	0.75164	85.30825	0.966173	48.69307	179.52	-1.15084	2.031596	7
46.60157	47.24052	92.89508	-26.421	183.818	43.83136	-2.52363	1.589851	6
-13.59	-5.24955	24.39548	-0.68877	-17.2954	-45.0942	-0.00598	0.627361	6
-17.6029	13.41057	10.66782	36.58551	-82.5216	31.31346	-2.97744	1.89597	7
-29.8968	13.4846	26.46422	1.507363	112.6223	10.08722	-1.94405	1.693566	6
-18.2203	92.6196	153.8688	0.966203	249.4967	-31.6483	-1.70886	1.296677	7
-36.1316	15.26726	13.5926	-2.39442	-98.3716	53.67466	-1.89186	2.008542	7
-32.6094	-7.19312	-23.782	-2.90944	-94.4912	-0.48619	-2.44242	1.7049	5

Table 2: MsPacman DQN boundary points: first 10 rows of features and action labels

Feature 1	Feature 2	Feature 3	Feature 4	Feature 5	Feature 6	Feature 7	Feature 8
0	0	0	0	55.7541	0	0	721.5164
0	0	0	0	0	0	0	55.56659
0	0	0	501.7624	0	0	0	336.9333
0	0	0	85.61454	0	0	0	431.6569
0	0	0	0	489.7511	0	0	1842.243
0	0	0	0	0	0	0	137.5602
0	0	0	0	0	0	0	830.2186
0	0	0	255.8091	0	0	0	336.7449
0	0	0	0	0	0	0	134.5811
0	0	0	0	0	0	0	321.8050

Feature 9	Feature 10	Feature 11	Feature 12	Feature 13	Feature 14	Feature 15	Feature 16	Action Label
0	0	318.1658	0	545.9904	84.66984	0	0	6
0	11.0026	0	304.9976	0	122.1123	0	0	2
300.3364	18.30009	207.49	0	457.2445	438.9895	0	0	7
180.606	132.7699	86.33698	81.04003	638.9478	276.7383	0	0	6
0	0	1569.231	0	275.1934	0	0	0	6
50.81373	59.32636	0	270.8656	28.70813	270.455	0	0	7
0	0	229.8056	0	536.8198	260.828	0	0	6
140.1302	42.31081	58.60357	0	670.4374	176.3808	0	0	7
0	30.09257	104.6578	0	0	299.6935	0	0	7
0	0	262.2588	0	50.81428	240.3015	0	0	5

Table 3: MsPacman DQN SHAP inverse boundary points: first 10 rows of features and action labels

Feature 1	Feature 2	Feature 3	Feature 4	Feature 5	Feature 6	Feature 7	Feature 8
0	-0.00083	-0.47892	1.12E-05	3.01E-05	0	0	0.058596
0	0.000949	-0.27889	-1.53E-05	1.98E-05	0	0	-0.1481
0	-0.00135	0.477397	-5.52E-08	6.72E-06	0	0	0.135079
0	-0.00022	0.081397	-2.44E-06	-1.36E-05	0	0	-0.29276
0	-0.00043	-0.24212	1.18E-05	7.31E-05	0	0	-0.29675
0	0.000124	2.800792	-2.25E-05	-8.00E-05	0	0	0.189882
0	-0.00087	-0.57139	1.17E-05	2.97E-05	0	0	0.039338
0	9.14E-05	3.346151	-3.30E-05	5.00E-06	0	0	0.127679
0	-0.0001	1.135439	-2.20E-05	3.00E-05	0	0	-0.50111
0	-0.00041	-0.2112	4.40E-06	1.48E-05	0	0	0.028318

Feature 9	Feature 10	Feature 11	Feature 12	Feature 13	Feature 14	Feature 15	Feature 16	Action Label
-0.00458	-0.28035	0.176815	-1.37E-05	0	-0.20625	0	0	5
0.179629	-0.16501	2.131016	0.000116	0	0.10562	0	0	7
-0.00406	0.423494	-1.38735	-1.44E-05	0	-0.00709	0	0	5
-0.0016	-0.46054	-0.36306	-4.85E-05	0	0.168933	0	0	5
-0.00646	0.14528	1.490529	6.42E-05	0	0.148152	0	0	5
0.001417	-0.01967	1.789025	8.46E-05	0	0.37831	0	0	8
-0.00475	-0.34087	0.33842	-1.48E-05	0	-0.19539	0	0	5
0.001948	-0.01433	1.796733	0.00011	0	0.671487	0	0	8
0.000805	-0.07721	3.341121	7.21E-05	0	0.606315	0	0	8
-0.0022	-0.01824	-0.36886	-1.40E-05	0	-0.16291	0	0	5

Table 4: MsPacman A2C boundary points: first 10 rows of features and action labels

Feature 1	Feature 2	Feature 3	Feature 4	Feature 5	Feature 6	Feature 7	Feature 8
0	0	623.6633	0	0	0	0	532.5274
0	0	653.3041	0	0	0	0	107.4317
0	0	1341.658	0	0	0	0	727.1529
0	0	1061.923	0	0	0	0	494.4895
0	0	616.0728	0	0	0	0	259.9639
0	0	478.1401	0	0	0	0	696.2931
0	0	583.0953	0	0	0	0	501.0357
0	0	384.8195	0	0	0	0	688.3864
0	0	710.8715	0	0	0	0	983.8112
0	0	568.2379	0	0	0	0	675.8421

Feature 9	Feature 10	Feature 11	Feature 12	Feature 13	Feature 14	Feature 15	Feature 16	Action Label
0	150.9219	601.0638	0	0	162.5402	0	0	5
87.21083	81.74716	0	0	0	0	0	0	7
0	668.9421	1414.396	0	0	64.81534	0	0	5
0	93.9263	1125.77	0	0	0	0	0	5
0	230.8709	124.3961	0	0	0	0	0	5
0	274.8654	1496.319	0	0	441.1012	0	0	8
0	121.8064	550.3	0	0	147.2741	0	0	5
0	166.9695	1494.9	0	0	517.485	0	0	8
0	330.6453	2159.496	0	0	576.4459	0	0	8
0	131.7175	958.8807	0	0	385.6672	0	0	5

Table 5: MsPacman A2C SHAP inverse boundary points: first 10 rows of features and action labels

Feature 1	Feature 2	Feature 3	Feature 4	Feature 5	Feature 6	Feature 7	Feature 8
0.000	-0.28516	0.000	0.072798	0.000265	0.000	0.000	0.000
0.000	-0.08226	0.000	0.378046	-0.00056	0.000	0.000	0.000
0.000	0.86831	0.000	0.295693	-0.00029	0.000	0.000	0.000
0.000	-0.58381	0.000	0.084519	-0.000063	0.000	0.000	0.000
0.000	-0.37113	0.000	-0.08261	-0.00043	0.000	0.000	0.000
0.000	-0.23301	0.000	-0.11092	-0.00054	0.000	0.000	0.000
0.000	-0.3258	0.000	0.177798	0.00016	0.000	0.000	0.000
0.000	-0.13854	0.000	-0.07107	-0.00072	0.000	0.000	0.000
0.000	-0.39994	0.000	-0.07986	-0.00044	0.000	0.000	0.000
0.000	0.147544	0.000	-0.07974	-0.00096	0.000	0.000	0.000

Feature 9	Feature 10	Feature 11	Feature 12	Feature 13	Feature 14	Feature 15	Feature 16	Action Label
0.000	-0.4569	-0.01058	2.505064	0.000	0.000	0.26214	0.000	7
0.000	0.34163	0.010641	1.282444	0.000	0.000	-0.04949	0.000	6
0.000	0.68037	0.010819	0.913588	0.000	0.000	-0.01256	0.000	6
0.000	-0.61006	-0.0000955	3.774243	0.000	0.000	-0.01605	0.000	7
0.000	-0.30679	0.004481	1.660903	0.000	0.000	0.040685	0.000	6
0.000	-0.33712	0.004529	1.43017	0.000	0.000	0.06036	0.000	6
0.000	-0.43532	-0.00619	2.333613	0.000	0.000	-0.03847	0.000	7
0.000	-0.49607	0.014154	2.157	0.000	0.000	0.012373	0.000	6
0.000	-0.64253	0.004522	1.725279	0.000	0.000	0.238071	0.000	6
0.000	-0.35632	0.015381	1.709701	0.000	0.000	0.350303	0.000	6

Table 6: MsPacman PPO boundary points: first 10 rows of features and action labels

Feature 1	Feature 2	Feature 3	Feature 4	Feature 5	Feature 6	Feature 7	Feature 8
0.0	5753.206	0.0	530.9578	0.0	0.0	0.0	0.0
0.0	6628.804	0.0	1914.645	0.0	0.0	0.0	0.0
0.0	0.000	0.0	2528.653	0.0	0.0	0.0	0.0
0.0	4611.498	0.0	550.1152	0.0	0.0	0.0	0.0
0.0	8737.567	0.0	0.000	0.0	0.0	0.0	0.0
0.0	7480.565	0.0	0.000	0.0	0.0	0.0	0.0
0.0	5501.599	0.0	33.12456	0.0	0.0	0.0	0.0
0.0	7509.492	0.0	0.000	0.0	0.0	0.0	0.0
0.0	8891.553	0.0	0.000	0.0	0.0	0.0	0.0
0.0	6040.661	0.0	0.000	0.0	0.0	0.0	0.0

Feature 9	Feature 10	Feature 11	Feature 12	Feature 13	Feature 14	Feature 15	Feature 16	Action Label
0.0	2318.034	0.0	8493.874	0.0	0.0	8382.263	0.0	7
0.0	1880.883	0.0	14349.77	0.0	0.0	11766.16	0.0	6
0.0	0.000	0.0	20786.43	0.0	0.0	9735.063	0.0	6
0.0	1762.912	0.0	6748.198	0.0	0.0	6996.48	0.0	7
0.0	6482.863	0.0	22678.59	0.0	0.0	3191.511	0.0	6
0.0	4270.52	0.0	17331.35	0.0	0.0	6207.685	0.0	6
0.0	2374.423	0.0	8500.413	0.0	0.0	7080.591	0.0	7
0.0	6573.165	0.0	29362.53	0.0	0.0	1421.398	0.0	6
0.0	6896.546	0.0	23498.77	0.0	0.0	3105.686	0.0	6
0.0	5298.294	0.0	23890.88	0.0	0.0	1742.465	0.0	6

Table 7: MsPacman PPO SHAP inverse boundary points: first 10 rows of features and action labels

Feature 1	Feature 2	Feature 3	Feature 4	Feature 5	Feature 6	Feature 7	Feature 8
5.474527	-0.81353	67.99976	-0.18912	-26.918	-0.15756	-1.73123	-10.2803
2.992853	2.733483	-3.56914	-0.13995	5.06779	0.207614	-3.64042	25.05078
1.108827	-0.73966	-10.4527	-0.04402	8.2174	-0.04362	-2.02183	-9.78841
12.07903	-0.79765	190.9837	-0.37814	3.13685	-0.28556	-2.23423	106.7969
10.21576	3.761232	68.81969	-0.36309	4.5211	-0.27273	-3.14379	86.7971
10.2965	-0.78144	74.93028	-0.32361	4.95804	-0.19189	-2.76325	86.90049
8.507568	8.391128	151.9825	-0.32951	12.85635	-0.34459	-4.24815	-17.8449
2.938708	-0.72215	26.80925	-0.13382	3.2263	-0.06201	-1.64585	-11.6016
15.82252	-0.84811	209.365	-0.43631	4.4694	-0.31842	-2.09036	125.2
4.299641	-0.94559	-7.29464	-0.18471	13.2794	-0.28606	14.64754	19.93434

Feature 9	Feature 10	Feature 11	Feature 12	Feature 13	Feature 14	Feature 15	Feature 16	Action Label
3.331623	-9.77	8.657984	315.9	28.0846	-1.42897	3.152705	0.0000242	8
0.443141	-5.35439	5.420255	0.539487	-14.8831	-0.15377	-7.97344	0.0000534	3
0.313884	-6.69001	1.645254	44.13974	-18.1456	-0.80795	-1.55171	0.0000535	8
3.305505	13.59553	16.9441	8.958751	-145.376	1.377216	34.02753	0.0000000	5
2.244834	58.93856	-1.35426	-3.01145	4.090079	-0.09288	-9.17819	0.0000379	8
1.037774	58.97981	13.57428	3.093952	-80.4599	3.308704	12.90698	0.0000372	6
3.216183	-13.9531	15.05736	49.27177	89.38817	-0.52471	11.5848	0.0000000	9
1.637403	-13.2263	5.023197	103.6954	-21.3427	5.47379	-8.87605	0.0000372	5
3.872871	-14.9694	20.44513	0.918966	-64.6853	1.795213	53.85848	0.0000000	8
-0.47081	-12.7496	6.945717	-7.97213	9.558705	3.580552	-8.14629	0.000129	3

Table 8: RoadRunner DQN boundary points: first 10 rows of features and action labels

Feature 1	Feature 2	Feature 3	Feature 4	Feature 5	Feature 6	Feature 7	Feature 8
0.000	0.000	188.7657	0.000	208.6209	0.000	0.000	0.000
0.000	13.94768	50.96701	0.000	18.80776	8.201801	0.000	60.99874
0.000	0.000	35.64004	0.000	105.0581	0.000	0.000	0.000
0.000	0.000	227.0123	0.000	95.6398	0.000	0.000	127.3856
0.000	14.1228	113.9336	0.000	49.6401	0.000	0.000	106.4597
0.000	0.000	138.5666	0.000	23.21588	0.000	0.000	110.8463
0.000	27.12692	207.4527	0.000	0.000	0.000	0.000	0.000
0.000	0.000	113.7223	0.000	128.9664	0.000	0.000	0.000
0.000	0.000	231.0666	0.000	101.2544	0.000	0.000	138.9797
0.000	0.000	42.31835	0.000	0.000	36.38669	0.000	53.29093

Feature 9	Feature 10	Feature 11	Feature 12	Feature 13	Feature 14	Feature 15	Feature 16	Action Label
0.000	0.000	0.000	604.8348	57.50573	0.000	0.000	0.000	8
0.000	21.39673	0.000	104.7776	110.2937	5.451507	0.000	0.000	3
0.000	0.000	0.000	196.1525	121.0192	0.000	0.000	0.000	8
0.000	186.7019	0.000	223.3806	273.6460	0.000	125.3206	0.000	5
0.000	114.6822	7.669223	84.23914	96.00603	6.905884	0.000	0.000	3
0.000	134.9267	0.000	204.6313	213.2327	0.000	221.8269	0.000	6
0.000	7.785656	0.000	237.4772	0.000	3.684652	0.000	0.000	9
0.000	0.000	0.000	285.1784	129.4608	53.5535	4.809501	0.000	8
0.000	219.5916	0.000	165.9190	180.7253	0.000	168.3602	0.000	5
0.000	0.000	0.000	81.0340	75.77461	0.000	9.164403	0.000	3

Table 9: RoadRunner DQN SHAP inverse boundary points: first 10 rows of features and action labels

Feature 1	Feature 2	Feature 3	Feature 4	Feature 5	Feature 6	Feature 7	Feature 8
-0.0016	0.012969	0.002574	0.006918	0.090507	0.004858	0.344943	4.097872
0.067005	0.111029	-0.00269	0.056097	0.010497	-0.0101	0.396967	2.144845
0.168133	0.205574	-0.00202	0.046697	-0.085069	-0.0076	0.334608	3.086863
0.251399	0.11519	-0.00046	0.061054	-1.47655	0.007191	0.419466	2.611407
0.172695	0.072814	0.001032	0.126251	2.13337	0.092112	0.115391	4.472525
0.117376	0.144224	-0.00195	0.032066	-2.19087	0.00218	0.313983	2.340529
0.057967	0.136672	-0.00153	-0.00688	-2.59928	0.00963	0.348639	2.715359
-0.00683	0.00922	0.001372	-0.021748	0.149261	0.028857	0.319187	5.202232
0.238766	1.495085	0.002403	0.017486	0.559244	0.006417	0.38527	1.023632
-1.22581	0.046178	-0.00249	0.054852	0.112022	-0.0097	-1.05545	1.078114

Feature 9	Feature 10	Feature 11	Feature 12	Feature 13	Feature 14	Feature 15	Feature 16	Action Label
-0.00038	0.193474	0.009643	0.021532	0.188902	0.044162	0.022337	0.328965	7
-0.00105	0.186545	0.011617	0.150055	0.042825	-0.77204	0.028056	0.107762	9
-0.00129	0.378642	0.009852	0.202114	0.154361	-0.79497	-0.02757	-1.49946	9
-0.00092	1.458449	0.021435	0.111257	0.220765	-0.51995	-0.00403	-0.45147	9
-0.00042	0.886021	-0.02182	0.314617	0.63647	0.347686	0.0359	-1.44858	2
-0.00008	0.033347	0.005236	0.12489	0.057393	-0.38435	-0.02944	-0.82626	9
-0.00013	0.112104	0.008091	0.155574	0.145118	-0.62689	-0.04284	-1.12652	9
-0.00018	0.272794	0.007354	-0.03508	0.13459	-0.02189	-0.01719	-0.19001	7
0.015837	0.64423	0.001668	-0.62335	2.441334	-1.68436	0.08042	0.177791	5
-0.0002	0.139825	-0.000057	-3.04481	0.041828	-1.05401	-0.00218	6.010482	9

Table 10: RoadRunner A2C boundary points: first 10 rows of features and action labels

Feature 1	Feature 2	Feature 3	Feature 4	Feature 5	Feature 6	Feature 7	Feature 8
161.505	0.000	0.000	0.000	849.9095	0.000	0.000	1037.385
95.19944	0.000	0.000	0.000	470.2562	0.000	0.000	0.000
66.96087	0.000	0.000	0.000	172.4873	0.000	6.232745	0.000
51.1582	50.33921	0.000	0.000	62.84172	237.3442	33.74626	936.9337
549.525	101.9358	0.000	0.000	104.4528	0.000	0.000	0.000
89.66468	0.000	0.000	0.000	93.95311	0.000	35.43744	0.000
131.0036	0.000	0.000	0.000	7.160192	0.000	54.5494	0.000
90.4573	0.000	0.000	0.000	132.6835	187.1228	0.000	2613.281
13.69985	847.7397	0.000	0.000	468.4573	19.38743	0.000	0.000
616.4103	0.000	0.000	0.000	180.913	0.000	645.9976	0.000

Feature 9	Feature 10	Feature 11	Feature 12	Feature 13	Feature 14	Feature 15	Feature 16	Action Label
0.000	440.8918	0.000	0.000	0.000	270.6354	56.48066	786.6356	7
0.000	180.0636	0.000	0.000	0.000	88.72929	96.3101	647.2335	9
0.000	171.6217	0.000	0.000	0.000	110.6941	0.000	181.6488	9
0.000	74.64204	55.82757	964.7496	246.0649	106.0566	0.000	317.4086	9
0.000	247.9345	0.000	0.000	0.000	157.3781	21.54585	1578.259	2
0.000	145.2424	0.000	0.000	0.000	45.90677	0.000	229.8769	9
0.000	486.9624	0.000	502.4604	0.000	159.6311	460.3797	1833.193	7
0.000	0.000	0.000	332.5967	611.1736	818.4494	531.9953	2331.473	5
0.000	0.000	0.000	1056.952	0.000	3.037189	0.000	3703.815	9

Table 11: RoadRunner A2C SHAP inverse boundary points: first 10 rows of features and action labels

Feature 1	Feature 2	Feature 3	Feature 4	Feature 5	Feature 6	Feature 7	Feature 8
-4.60653	0.296192	0.969315	0.000136	0.08256	0.000	2.431848	0.011123
0.727034	0.678398	1.124768	-0.000008	1.15713	0.000	0.155846	-0.00254
0.177717	0.13062	-0.09505	-0.00013	0.01159	0.000	0.778338	-0.00021
0.301813	0.12316	0.271282	-0.00018	0.03311	0.000	0.486024	0.011636
0.414713	-0.20925	1.222974	0.000054	0.10786	0.000	0.251595	-0.01727
1.700075	0.199318	0.225426	-0.000032	0.01006	0.000	0.652782	0.030314
-0.25459	0.132821	0.956079	0.000060	0.05553	0.000	-0.37312	-0.00054
-2.25543	-0.25148	-0.92031	-0.000032	0.07573	0.000	1.738408	0.027718
0.318616	0.097084	0.13207	-0.00012	0.16962	0.000	0.686528	0.01671
0.680373	0.126166	-0.27959	-0.00014	0.04886	0.000	0.034872	0.012065

Feature 9	Feature 10	Feature 11	Feature 12	Feature 13	Feature 14	Feature 15	Feature 16	Action Label
0.736442	-0.26678	0.000	-0.37522	0.034589	0.000	0.039715	0.060039	7
-0.11608	-1.53109	0.000	-0.33782	0.695403	0.000	-0.00257	-0.01403	17
0.492757	-0.06871	0.000	1.107499	0.237301	0.000	0.008528	0.034149	7
0.143643	0.03569	0.000	0.77755	0.199367	0.000	0.00316	0.029548	7
0.018323	-0.032362	0.000	1.897528	-0.05634	0.000	-0.00535	0.043167	2
0.033747	-0.42868	0.000	1.678755	0.028648	0.000	0.026876	0.021954	9
-0.33624	0.12832	0.000	-0.94617	-0.06385	0.000	0.009777	0.102698	7
-0.22714	0.32757	0.000	2.441481	-0.37498	0.000	0.03634	0.068526	7
0.168505	-0.14289	0.000	0.88648	0.167437	0.000	0.00311	0.029505	7
-0.32175	-0.07368	0.000	1.56611	-0.84533	0.000	0.000639	0.02832	7

Table 12: RoadRunner PPO boundary points: first 10 rows of features and action labels

Feature 1	Feature 2	Feature 3	Feature 4	Feature 5	Feature 6	Feature 7	Feature 8
393.7799	0.000	710.9127	0.000	0.000	0.000	706.2158	0.000
0.000	16696.2	19701.97	0.000	0.000	0.000	1955.914	0.000
1478.477	0.000	2021.436	0.000	0.000	0.000	727.3788	60.47329
1949.78	0.000	440.0298	0.000	404.4525	0.000	883.1434	0.000
1911.436	380.9045	242.8682	0.000	440.9319	0.000	1777.836	0.000
2592.608	0.000	1427.355	0.000	0.000	0.000	1441.367	0.000
1252.199	76.16316	441.7511	0.000	0.000	0.000	2203.14	0.000
595.1301	804.1888	2465.322	0.000	0.000	0.000	657.2477	0.000
1740.248	662.2636	1100.283	0.000	136.821	0.000	922.0039	0.000
2394.39	496.4578	2170.893	0.000	20.7365	0.000	1717.301	0.000

Feature 9	Feature 10	Feature 11	Feature 12	Feature 13	Feature 14	Feature 15	Feature 16	Action Label
135.8958	234.148	0.000	405.4395	74.99923	0.000	0.000	38.39702	7
0.000	467.3831	0.000	2348.284	3777.795	0.000	0.000	0.000	17
0.000	581.9508	0.000	1589.511	0.000	0.000	0.000	0.000	7
511.5791	771.8015	0.000	1301.291	46.28678	0.000	63.36972	0.000	7
1008.254	396.2003	0.000	1213.938	742.5882	0.000	0.000	0.000	2
327.657	813.8804	0.000	308.6375	461.7389	0.000	0.000	0.000	9
911.6214	491.1194	0.000	385.752	611.6022	0.000	0.000	0.000	7
935.967	95.45456	0.000	1446.708	759.0374	0.000	0.000	0.000	7
413.0294	505.3461	0.000	1325.548	217.6241	0.000	83.9481	0.000	7
1186.176	474.8096	0.000	1641.388	1450.506	0.000	0.000	0.000	7

Table 13: RoadRunner PPO SHAP inverse boundary points: first 10 rows of features and action labels

Appendix F: Decision Trees

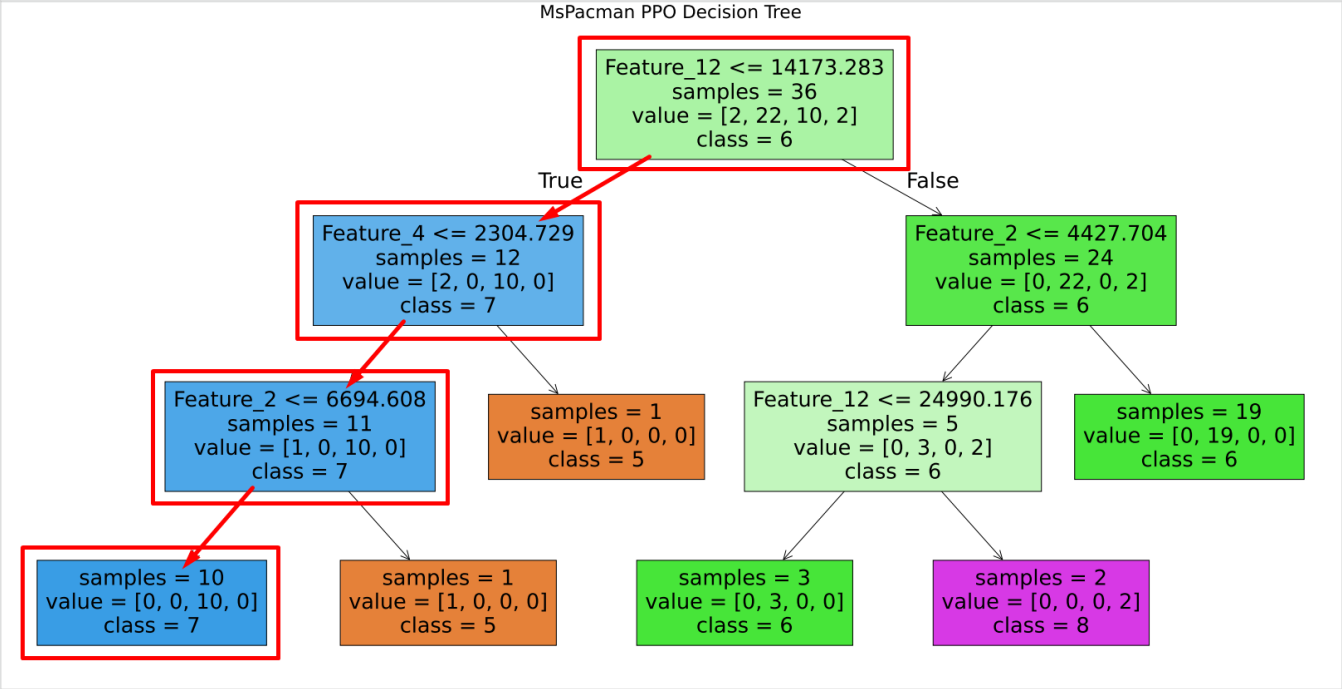

Figure 10: MsPacman PPO decision tree

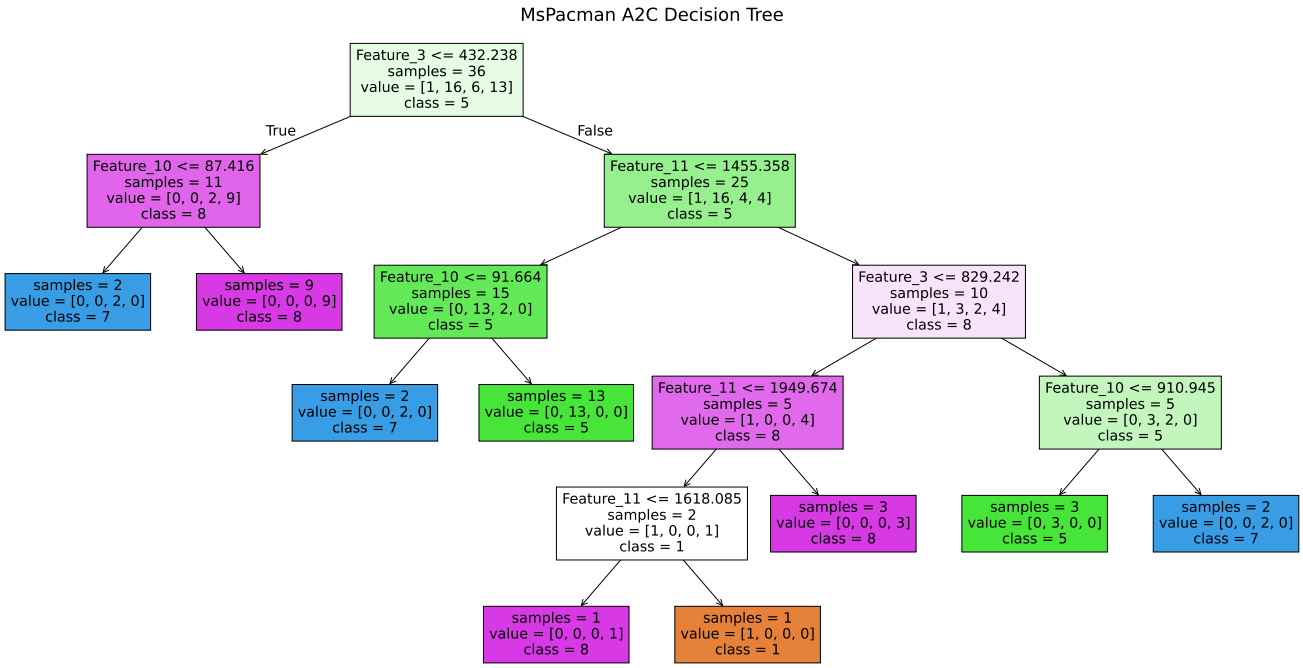

Figure 11: MsPacman A2C decision tree

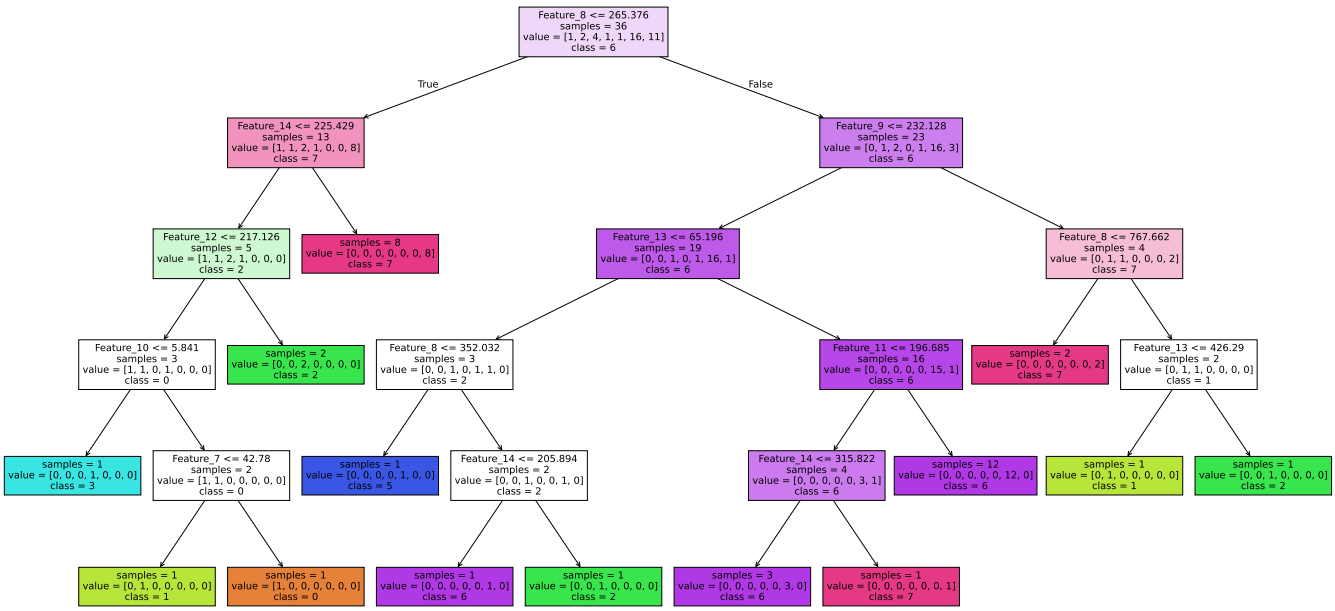

Figure 12: MsPacman DQN decision tree

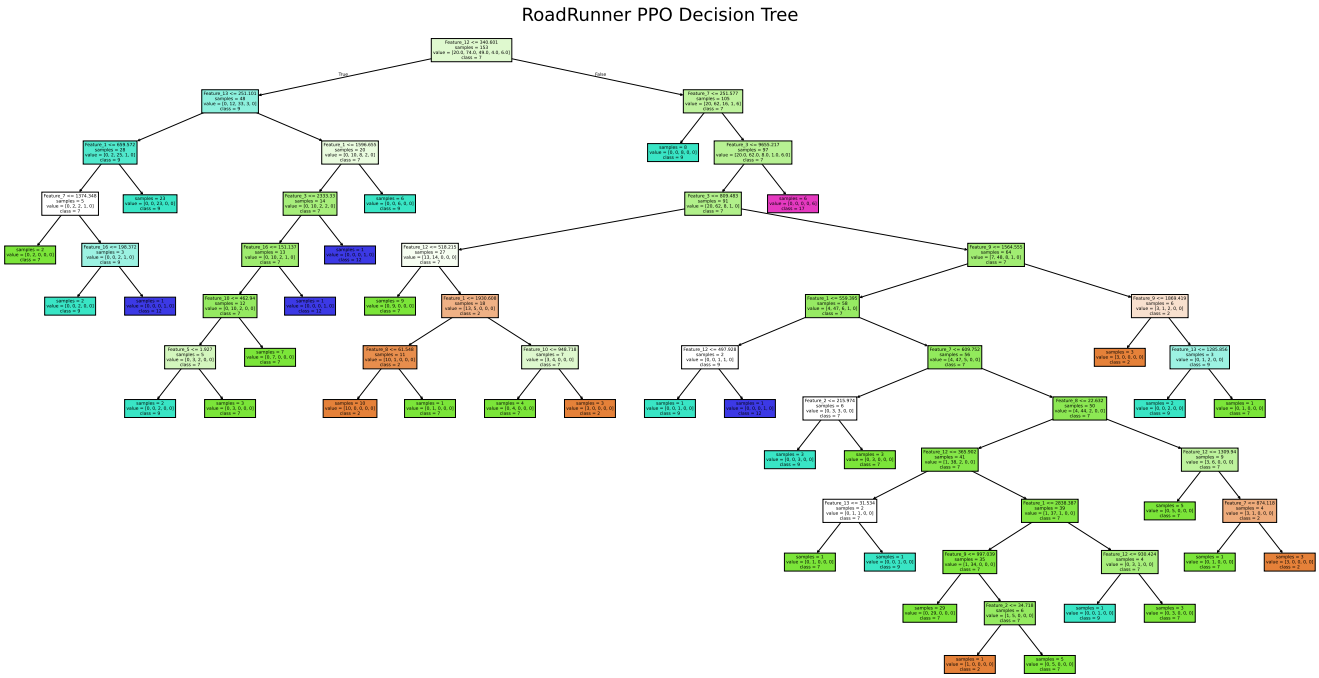

Figure 13: RoadRunner PPO decision tree

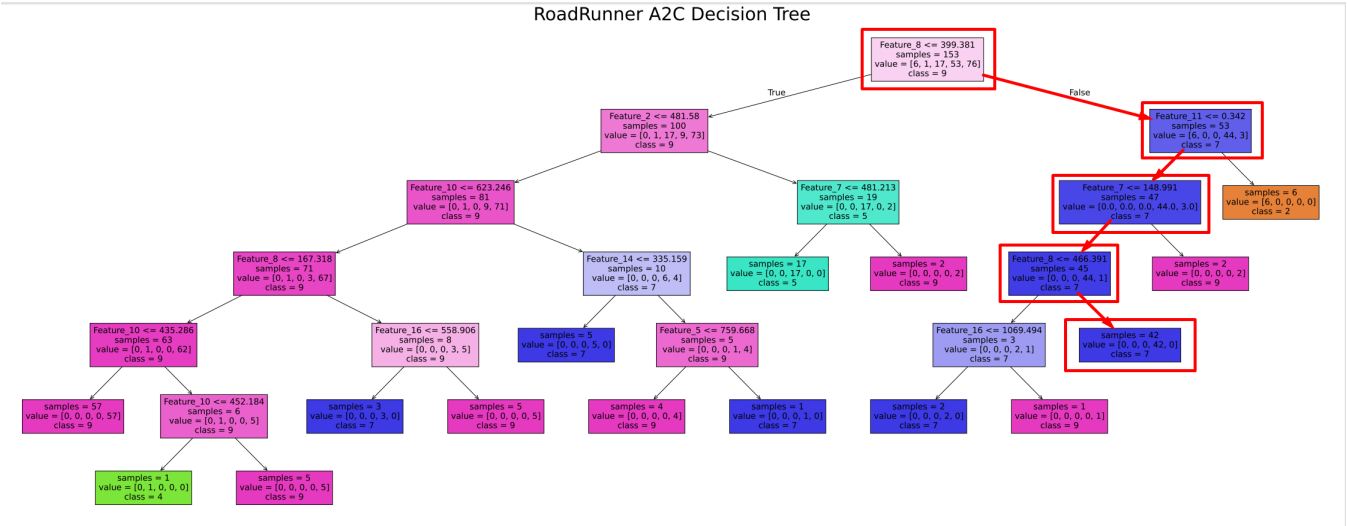

Figure 14: RoadRunner A2C decision tree

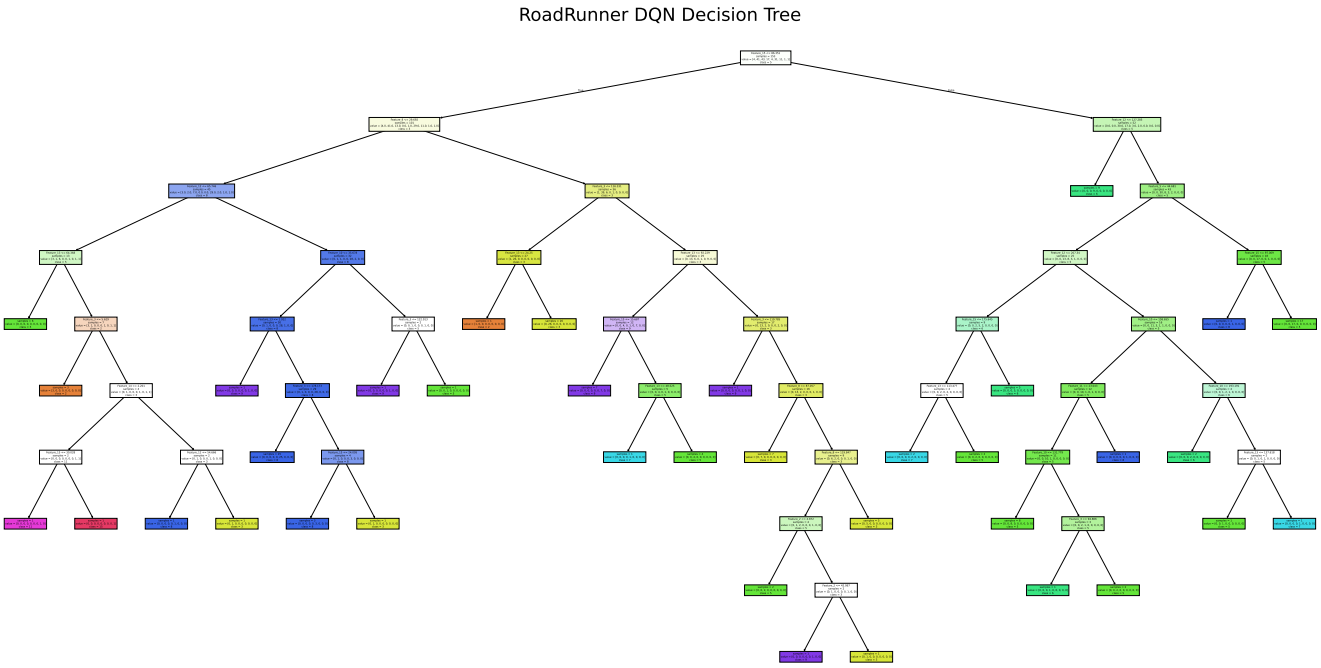

Figure 15: RoadRunner DQN decision tree

Appendix G: Linear Regression

Algorithm	Decision Boundary
PPO	$f(x) = 7.37 + 2.77 \times 10^{-4} \cdot x_2 - 1.94 \times 10^{-4} \cdot x_4 - 8.30 \times 10^{-3} \cdot x_5$ $- 1.58 \times 10^{-3} \cdot x_7 - 5.66 \times 10^{-4} \cdot x_{10} + 1.29 \times 10^{-3} \cdot x_{11}$ $+ 1.29 \times 10^{-5} \cdot x_{12} - 1.35 \times 10^{-4} \cdot x_{15}$
A2C	$f(x) = 4.95 + 4.05 \times 10^{-3} \cdot x_3 - 7.39 \times 10^{-3} \cdot x_8 + 4.76 \times 10^{-3} \cdot x_9$ $- 6.18 \times 10^{-3} \cdot x_{10} + 3.51 \times 10^{-3} \cdot x_{11} + 3.47 \times 10^{-3} \cdot x_{14}$
DQN	$f(x) = 6.17 - 1.08 \times 10^{-3} \cdot x_1 + 5.24 \times 10^{-2} \cdot x_2 + 1.11 \times 10^{-3} \cdot x_3$ $+ 4.34 \times 10^{-3} \cdot x_4 + 3.12 \times 10^{-3} \cdot x_5 - 5.98 \times 10^{-2} \cdot x_6 - 6.91 \times 10^{-2} \cdot x_7$ $+ 2.14 \times 10^{-3} \cdot x_8 - 4.70 \times 10^{-3} \cdot x_9 - 9.94 \times 10^{-4} \cdot x_{10} - 3.79 \times 10^{-3} \cdot x_{11}$ $- 2.10 \times 10^{-3} \cdot x_{12} - 1.33 \times 10^{-3} \cdot x_{13} - 3.45 \times 10^{-5} \cdot x_{14} - 1.50 \times 10^{-3} \cdot x_{15}$ $- 4.89 \times 10^{-3} \cdot x_{16}$

Table 14: MsPacman: interpretable policy boundary for linear regression

Algorithm	Decision Boundary
PPO	$f(x) = 6.85 + 9.21 \times 10^{-4} \cdot x_1 - 3.57 \times 10^{-4} \cdot x_2 + 1.14 \times 10^{-3} \cdot x_3 - 4.51 \times 10^{-6} \cdot x_5$ $- 4.72 \times 10^{-4} \cdot x_7 + 1.59 \times 10^{-3} \cdot x_8 + 1.81 \times 10^{-4} \cdot x_9 - 2.66 \times 10^{-4} \cdot x_{10}$ $- 2.73 \times 10^{-3} \cdot x_{12} - 2.05 \times 10^{-5} \cdot x_{13} + 3.23 \times 10^{-3} \cdot x_{15} + 2.21 \times 10^{-3} \cdot x_{16}$
A2C	$f(x) = 8.82 - 9.00 \times 10^{-4} \cdot x_1 - 5.92 \times 10^{-3} \cdot x_2 + 1.77 \times 10^{-3} \cdot x_3 - 9.55 \times 10^{-3} \cdot x_4$ $- 6.94 \times 10^{-4} \cdot x_5 - 4.30 \times 10^{-3} \cdot x_6 + 1.03 \times 10^{-4} \cdot x_7 - 9.70 \times 10^{-4} \cdot x_8$ $+ 1.42 \times 10^{-2} \cdot x_9 - 1.03 \times 10^{-3} \cdot x_{10} - 4.23 \times 10^{-3} \cdot x_{11} - 2.10 \times 10^{-3} \cdot x_{12}$ $- 1.02 \times 10^{-4} \cdot x_{13} - 4.19 \times 10^{-4} \cdot x_{14} + 1.34 \times 10^{-3} \cdot x_{15} + 1.08 \times 10^{-3} \cdot x_{16}$
DQN	$f(x) = 6.12 + 8.52 \times 10^{-3} \cdot x_1 - 3.26 \times 10^{-2} \cdot x_2 - 3.48 \times 10^{-3} \cdot x_3 + 4.69 \times 10^{-3} \cdot x_4$ $- 3.78 \times 10^{-3} \cdot x_5 - 5.54 \times 10^{-2} \cdot x_6 + 2.44 \times 10^{-2} \cdot x_7 - 2.91 \times 10^{-2} \cdot x_8$ $+ 3.47 \times 10^{-3} \cdot x_9 + 1.87 \times 10^{-2} \cdot x_{10} - 5.53 \times 10^{-3} \cdot x_{11} + 6.60 \times 10^{-3} \cdot x_{12}$ $- 2.96 \times 10^{-3} \cdot x_{13} + 1.75 \times 10^{-3} \cdot x_{14} - 4.66 \times 10^{-3} \cdot x_{15}$

Table 15: RoadRunner: interpretable policy boundary for linear regression

Appendix H: Logistic Regression

Action i	$f_i(x)$
5	$2.21 \times 10^{-7} + 9.61 \times 10^{-4} x_2 + 1.69 \times 10^{-4} x_4 - 9.86 \times 10^{-7} x_5 + 1.27 \times 10^{-3} x_7 + 8.61 \times 10^{-4} x_{10} + 3.03 \times 10^{-4} x_{11} - 4.15 \times 10^{-4} x_{12} - 7.49 \times 10^{-5} x_{15}$
6	$-1.14 \times 10^{-7} - 2.17 \times 10^{-3} x_2 + 2.28 \times 10^{-3} x_4 - 4.62 \times 10^{-7} x_5 - 8.96 \times 10^{-4} x_7 + 1.08 \times 10^{-3} x_{10} - 2.40 \times 10^{-4} x_{11} + 1.17 \times 10^{-3} x_{12} - 4.35 \times 10^{-4} x_{15}$
7	$6.06 \times 10^{-7} + 1.90 \times 10^{-3} x_2 - 1.47 \times 10^{-3} x_4 + 1.58 \times 10^{-6} x_5 - 3.68 \times 10^{-4} x_7 + 1.11 \times 10^{-3} x_{10} - 5.90 \times 10^{-5} x_{11} - 2.23 \times 10^{-3} x_{12} + 1.75 \times 10^{-3} x_{15}$
8	$-7.12 \times 10^{-7} - 6.93 \times 10^{-4} x_2 - 9.76 \times 10^{-4} x_4 - 1.30 \times 10^{-7} x_5 - 9.69 \times 10^{-6} x_7 - 3.05 \times 10^{-3} x_{10} - 4.47 \times 10^{-6} x_{11} + 1.47 \times 10^{-3} x_{12} - 1.23 \times 10^{-3} x_{15}$

Table 16: MsPacman PPO: interpretable policy boundary for logistic regression

Action i	$f_i(x)$
1	$-4.54 \times 10^{-5} - 6.57 \times 10^{-3} x_3 + 8.94 \times 10^{-3} x_8 - 8.20 \times 10^{-5} x_9 + 6.73 \times 10^{-3} x_{10} - 4.47 \times 10^{-3} x_{11} + 6.11 \times 10^{-3} x_{14}$
5	$6.59 \times 10^{-5} + 9.31 \times 10^{-3} x_3 + 2.13 \times 10^{-2} x_8 - 7.33 \times 10^{-3} x_9 + 3.39 \times 10^{-3} x_{10} - 1.33 \times 10^{-2} x_{11} - 6.96 \times 10^{-3} x_{14}$
7	$-2.49 \times 10^{-5} + 1.62 \times 10^{-2} x_3 - 1.46 \times 10^{-2} x_8 + 7.45 \times 10^{-3} x_9 - 5.94 \times 10^{-3} x_{10} + 1.26 \times 10^{-3} x_{11} + 6.96 \times 10^{-4} x_{14}$
8	$4.39 \times 10^{-6} - 1.89 \times 10^{-2} x_3 - 1.57 \times 10^{-2} x_8 - 3.56 \times 10^{-5} x_9 - 4.18 \times 10^{-3} x_{10} + 1.66 \times 10^{-2} x_{11} + 1.57 \times 10^{-4} x_{14}$

Table 17: MsPacman A2C: interpretable policy boundary for logistic regression

Action i	$f_i(x)$
0	$9.37 \times 10^{-5} - 2.29 \times 10^{-4} x_1 - 7.40 \times 10^{-5} x_2 - 7.46 \times 10^{-5} x_3 - 1.48 \times 10^{-3} x_4 - 1.61 \times 10^{-4} x_5 - 3.56 \times 10^{-4} x_6 + 2.29 \times 10^{-2} x_7 - 1.61 \times 10^{-2} x_8 - 3.53 \times 10^{-3} x_9 - 8.99 \times 10^{-3} x_{10} - 4.98 \times 10^{-3} x_{11} + 4.51 \times 10^{-3} x_{12} - 3.42 \times 10^{-3} x_{13} + 1.51 \times 10^{-2} x_{14} - 5.62 \times 10^{-5} x_{15} - 1.03 \times 10^{-3} x_{16}$
1	$1.50 \times 10^{-5} - 2.97 \times 10^{-4} x_1 - 9.49 \times 10^{-4} x_2 - 2.25 \times 10^{-4} x_3 - 5.42 \times 10^{-3} x_4 - 2.22 \times 10^{-3} x_5 + 9.06 \times 10^{-3} x_6 - 3.71 \times 10^{-4} x_7 + 8.84 \times 10^{-3} x_8 + 2.66 \times 10^{-2} x_9 + 7.08 \times 10^{-3} x_{10} - 7.55 \times 10^{-3} x_{11} - 1.09 \times 10^{-2} x_{12} + 4.77 \times 10^{-5} x_{13} - 1.05 \times 10^{-2} x_{14} - 1.50 \times 10^{-2} x_{15} - 1.34 \times 10^{-3} x_{16}$
2	$-1.06 \times 10^{-4} + 1.05 \times 10^{-3} x_1 - 1.10 \times 10^{-4} x_2 - 2.38 \times 10^{-4} x_3 - 2.91 \times 10^{-3} x_4 - 5.65 \times 10^{-3} x_5 + 1.32 \times 10^{-4} x_6 - 5.77 \times 10^{-3} x_7 - 1.29 \times 10^{-2} x_8 - 2.81 \times 10^{-3} x_9 + 8.72 \times 10^{-3} x_{10} + 2.47 \times 10^{-2} x_{11} + 1.65 \times 10^{-2} x_{12} - 9.90 \times 10^{-3} x_{13} + 1.78 \times 10^{-3} x_{14} + 2.02 \times 10^{-2} x_{15} + 4.76 \times 10^{-3} x_{16}$
3	$-2.32 \times 10^{-5} - 9.31 \times 10^{-5} x_1 - 8.10 \times 10^{-5} x_2 + 1.04 \times 10^{-2} x_3 - 1.94 \times 10^{-3} x_4 + 4.20 \times 10^{-3} x_5 - 4.29 \times 10^{-4} x_6 - 3.89 \times 10^{-4} x_7 - 8.58 \times 10^{-3} x_8 - 2.01 \times 10^{-3} x_9 - 1.65 \times 10^{-3} x_{10} + 8.15 \times 10^{-3} x_{11} - 3.12 \times 10^{-3} x_{12} + 7.88 \times 10^{-3} x_{13} - 7.57 \times 10^{-3} x_{14} - 1.10 \times 10^{-4} x_{15} - 4.20 \times 10^{-4} x_{16}$
5	$1.50 \times 10^{-4} - 6.85 \times 10^{-5} x_1 - 2.54 \times 10^{-4} x_2 - 1.30 \times 10^{-4} x_3 - 4.34 \times 10^{-3} x_4 - 3.80 \times 10^{-3} x_5 - 6.65 \times 10^{-4} x_6 - 1.06 \times 10^{-3} x_7 + 3.67 \times 10^{-3} x_8 - 1.07 \times 10^{-2} x_9 - 3.67 \times 10^{-3} x_{10} + 4.52 \times 10^{-3} x_{11} - 6.73 \times 10^{-3} x_{12} + 5.65 \times 10^{-3} x_{13} + 1.72 \times 10^{-3} x_{14} - 5.14 \times 10^{-3} x_{15} - 3.09 \times 10^{-4} x_{16}$
6	$-8.05 \times 10^{-5} - 7.67 \times 10^{-5} x_1 + 9.98 \times 10^{-3} x_2 - 9.69 \times 10^{-3} x_3 + 6.58 \times 10^{-3} x_4 + 3.64 \times 10^{-3} x_5 + 4.22 \times 10^{-3} x_6 - 2.66 \times 10^{-4} x_7 + 7.39 \times 10^{-3} x_8 - 1.75 \times 10^{-2} x_9 - 2.85 \times 10^{-4} x_{10} + 8.63 \times 10^{-3} x_{11} + 2.29 \times 10^{-3} x_{12} + 1.94 \times 10^{-2} x_{13} - 2.01 \times 10^{-2} x_{14} - 1.13 \times 10^{-2} x_{15} - 3.46 \times 10^{-4} x_{16}$
7	$-4.95 \times 10^{-5} - 2.91 \times 10^{-4} x_1 - 8.51 \times 10^{-3} x_2 - 6.61 \times 10^{-5} x_3 + 9.50 \times 10^{-3} x_4 + 3.99 \times 10^{-3} x_5 - 1.20 \times 10^{-2} x_6 - 1.51 \times 10^{-2} x_7 + 1.77 \times 10^{-2} x_8 + 9.91 \times 10^{-3} x_9 - 1.22 \times 10^{-3} x_{10} - 3.35 \times 10^{-2} x_{11} - 2.57 \times 10^{-3} x_{12} - 1.97 \times 10^{-2} x_{13} + 1.95 \times 10^{-2} x_{14} + 1.14 \times 10^{-2} x_{15} - 1.31 \times 10^{-3} x_{16}$

Table 18: MsPacman DQN: interpretable policy boundary for logistic regression

Action i	$f_i(x)$
2	$-5.32 \times 10^{-6} - 2.45 \times 10^{-3} x_1 - 6.40 \times 10^{-4} x_2 - 4.97 \times 10^{-3} x_3 - 2.69 \times 10^{-4} x_5 + 2.25 \times 10^{-3} x_7 - 2.26 \times 10^{-7} x_8 - 4.24 \times 10^{-4} x_9 - 8.58 \times 10^{-4} x_{10} + 9.71 \times 10^{-3} x_{12} + 1.69 \times 10^{-3} x_{13} + 3.58 \times 10^{-4} x_{15} - 1.90 \times 10^{-4} x_{16}$
7	$6.16 \times 10^{-6} + 2.72 \times 10^{-3} x_1 + 5.40 \times 10^{-4} x_2 - 1.87 \times 10^{-4} x_3 - 8.33 \times 10^{-6} x_5 + 5.53 \times 10^{-4} x_7 - 3.31 \times 10^{-4} x_8 - 9.47 \times 10^{-4} x_9 + 8.05 \times 10^{-4} x_{10} + 1.88 \times 10^{-3} x_{12} - 5.16 \times 10^{-4} x_{13} - 4.61 \times 10^{-4} x_{15} - 5.13 \times 10^{-4} x_{16}$
9	$2.92 \times 10^{-6} + 5.07 \times 10^{-3} x_1 - 1.63 \times 10^{-3} x_2 + 3.06 \times 10^{-3} x_3 + 5.36 \times 10^{-4} x_5 - 3.27 \times 10^{-3} x_7 + 6.30 \times 10^{-4} x_8 + 2.57 \times 10^{-3} x_9 + 1.44 \times 10^{-3} x_{10} - 8.63 \times 10^{-3} x_{12} - 1.69 \times 10^{-3} x_{13} + 1.53 \times 10^{-4} x_{15} + 4.53 \times 10^{-5} x_{16}$
12	$-1.73 \times 10^{-6} - 3.51 \times 10^{-3} x_1 - 1.48 \times 10^{-4} x_2 + 1.69 \times 10^{-3} x_3 - 1.99 \times 10^{-4} x_5 + 2.07 \times 10^{-3} x_7 - 2.59 \times 10^{-4} x_8 - 3.22 \times 10^{-4} x_9 - 1.08 \times 10^{-3} x_{10} - 2.16 \times 10^{-3} x_{12} + 5.44 \times 10^{-4} x_{13} - 3.16 \times 10^{-5} x_{15} + 7.63 \times 10^{-4} x_{16}$
17	$-2.03 \times 10^{-6} - 1.83 \times 10^{-3} x_1 + 1.88 \times 10^{-3} x_2 + 4.05 \times 10^{-4} x_3 - 5.99 \times 10^{-5} x_5 - 1.60 \times 10^{-3} x_7 - 3.94 \times 10^{-5} x_8 - 8.73 \times 10^{-4} x_9 - 3.05 \times 10^{-4} x_{10} - 8.01 \times 10^{-4} x_{12} - 1.89 \times 10^{-5} x_{13} - 1.76 \times 10^{-5} x_{15} - 1.06 \times 10^{-4} x_{16}$

Table 19: RoadRunner PPO: interpretable policy boundary for logistic regression

Action i	$f_i(x)$
2	$-2.86 \times 10^{-6} - 1.35 \times 10^{-3} x_1 + 1.61 \times 10^{-3} x_2 - 1.98 \times 10^{-5} x_3 + 1.56 \times 10^{-3} x_4 - 1.17 \times 10^{-2} x_5 + 3.76 \times 10^{-3} x_6 - 6.08 \times 10^{-4} x_7 + 1.83 \times 10^{-2} x_8 - 3.67 \times 10^{-6} x_9 - 1.45 \times 10^{-3} x_{10} + 2.28 \times 10^{-3} x_{11} + 8.55 \times 10^{-3} x_{12} + 6.14 \times 10^{-3} x_{13} - 2.22 \times 10^{-3} x_{14} - 2.16 \times 10^{-3} x_{15} - 8.77 \times 10^{-3} x_{16}$
4	$-5.35 \times 10^{-5} + 3.34 \times 10^{-3} x_1 - 1.96 \times 10^{-3} x_2 - 6.08 \times 10^{-4} x_3 - 6.50 \times 10^{-5} x_4 + 4.06 \times 10^{-3} x_5 - 1.04 \times 10^{-3} x_6 + 2.62 \times 10^{-3} x_7 - 5.72 \times 10^{-3} x_8 - 7.24 \times 10^{-6} x_9 + 3.40 \times 10^{-3} x_{10} - 3.75 \times 10^{-5} x_{11} - 4.91 \times 10^{-3} x_{12} - 2.44 \times 10^{-3} x_{13} - 6.74 \times 10^{-3} x_{14} - 1.03 \times 10^{-3} x_{15} + 3.41 \times 10^{-3} x_{16}$
5	$-2.82 \times 10^{-5} - 7.23 \times 10^{-3} x_1 + 1.14 \times 10^{-2} x_2 - 1.97 \times 10^{-5} x_3 - 1.84 \times 10^{-5} x_4 - 6.60 \times 10^{-3} x_5 - 1.41 \times 10^{-3} x_6 - 6.26 \times 10^{-3} x_7 - 8.87 \times 10^{-3} x_8 + 2.14 \times 10^{-5} x_9 - 7.41 \times 10^{-3} x_{10} - 5.33 \times 10^{-5} x_{11} - 3.18 \times 10^{-3} x_{12} + 7.26 \times 10^{-3} x_{13} + 1.81 \times 10^{-3} x_{14} + 2.15 \times 10^{-3} x_{15} + 3.50 \times 10^{-3} x_{16}$
7	$-1.50 \times 10^{-4} - 2.88 \times 10^{-3} x_1 + 2.75 \times 10^{-3} x_2 - 7.10 \times 10^{-4} x_3 - 1.06 \times 10^{-3} x_4 + 1.15 \times 10^{-2} x_5 + 1.82 \times 10^{-3} x_6 + 8.55 \times 10^{-3} x_7 + 1.14 \times 10^{-2} x_8 - 4.94 \times 10^{-5} x_9 + 6.46 \times 10^{-3} x_{10} - 1.96 \times 10^{-3} x_{11} + 1.15 \times 10^{-2} x_{12} + 1.57 \times 10^{-3} x_{13} - 3.53 \times 10^{-3} x_{14} + 1.96 \times 10^{-3} x_{15} - 7.76 \times 10^{-3} x_{16}$
9	$2.34 \times 10^{-4} + 8.11 \times 10^{-3} x_1 - 1.38 \times 10^{-2} x_2 + 1.36 \times 10^{-3} x_3 - 4.17 \times 10^{-4} x_4 + 2.76 \times 10^{-3} x_5 - 3.13 \times 10^{-3} x_6 - 4.31 \times 10^{-3} x_7 - 1.51 \times 10^{-2} x_8 + 3.89 \times 10^{-5} x_9 - 9.97 \times 10^{-4} x_{10} - 2.26 \times 10^{-4} x_{11} - 1.20 \times 10^{-2} x_{12} - 1.25 \times 10^{-2} x_{13} + 1.07 \times 10^{-2} x_{14} - 9.17 \times 10^{-4} x_{15} + 9.62 \times 10^{-3} x_{16}$

Table 20: RoadRunner A2C: interpretable policy boundary for logistic regression

Action i	$f_i(x)$
2	$-3.21 \times 10^{-4} - 2.84 \times 10^{-3} x_1 + 6.14 \times 10^{-3} x_2 + 2.54 \times 10^{-3} x_3 - 5.52 \times 10^{-4} x_4 - 1.67 \times 10^{-2} x_5 + 9.15 \times 10^{-3} x_6 + 7.05 \times 10^{-2} x_7 + 1.98 \times 10^{-2} x_8 - 3.41 \times 10^{-3} x_9 - 1.92 \times 10^{-2} x_{10} - 3.83 \times 10^{-3} x_{11} - 3.61 \times 10^{-2} x_{12} + 3.10 \times 10^{-2} x_{13} - 7.27 \times 10^{-3} x_{14} + 1.95 \times 10^{-2} x_{15}$
3	$3.29 \times 10^{-3} - 2.14 \times 10^{-2} x_1 + 4.69 \times 10^{-2} x_2 + 1.04 \times 10^{-2} x_3 - 4.94 \times 10^{-3} x_4 + 1.05 \times 10^{-2} x_5 + 1.40 \times 10^{-2} x_6 + 9.10 \times 10^{-3} x_7 + 4.96 \times 10^{-3} x_8 + 1.89 \times 10^{-2} x_9 - 1.79 \times 10^{-3} x_{10} - 6.09 \times 10^{-3} x_{11} + 2.87 \times 10^{-2} x_{12} + 1.80 \times 10^{-2} x_{13} - 8.07 \times 10^{-3} x_{14} - 4.53 \times 10^{-2} x_{15}$
5	$-3.82 \times 10^{-3} + 1.38 \times 10^{-2} x_1 - 2.11 \times 10^{-2} x_2 + 5.82 \times 10^{-3} x_3 - 4.63 \times 10^{-3} x_4 + 3.23 \times 10^{-2} x_5 - 7.31 \times 10^{-3} x_6 - 3.31 \times 10^{-2} x_7 + 1.94 \times 10^{-2} x_8 + 7.67 \times 10^{-3} x_9 - 2.10 \times 10^{-2} x_{10} + 2.40 \times 10^{-2} x_{11} + 3.09 \times 10^{-2} x_{12} - 1.02 \times 10^{-2} x_{13} - 6.90 \times 10^{-3} x_{14} + 2.54 \times 10^{-2} x_{15}$
6	$-2.42 \times 10^{-4} + 5.95 \times 10^{-4} x_1 - 2.69 \times 10^{-3} x_2 - 1.15 \times 10^{-2} x_3 - 5.70 \times 10^{-4} x_4 - 1.82 \times 10^{-2} x_5 - 2.29 \times 10^{-3} x_6 - 1.28 \times 10^{-2} x_7 + 1.02 \times 10^{-2} x_8 + 6.67 \times 10^{-3} x_9 + 3.24 \times 10^{-2} x_{10} - 8.66 \times 10^{-4} x_{11} - 4.73 \times 10^{-2} x_{12} - 2.27 \times 10^{-2} x_{13} + 2.38 \times 10^{-3} x_{14} + 9.63 \times 10^{-2} x_{15}$
7	$-1.45 \times 10^{-3} - 1.09 \times 10^{-3} x_1 - 1.09 \times 10^{-2} x_2 - 1.22 \times 10^{-2} x_3 - 1.40 \times 10^{-3} x_4 - 3.52 \times 10^{-2} x_5 - 8.33 \times 10^{-3} x_6 - 4.28 \times 10^{-2} x_7 + 3.76 \times 10^{-2} x_8 - 3.87 \times 10^{-3} x_9 + 2.25 \times 10^{-2} x_{10} - 2.47 \times 10^{-3} x_{11} + 1.18 \times 10^{-2} x_{12} - 5.57 \times 10^{-2} x_{13} - 1.46 \times 10^{-2} x_{14} + 4.74 \times 10^{-2} x_{15}$
8	$2.05 \times 10^{-3} + 1.61 \times 10^{-2} x_1 - 2.26 \times 10^{-2} x_2 - 3.22 \times 10^{-2} x_3 + 1.28 \times 10^{-2} x_4 + 2.20 \times 10^{-2} x_5 - 9.96 \times 10^{-5} x_6 - 9.35 \times 10^{-3} x_7 - 6.44 \times 10^{-2} x_8 + 2.68 \times 10^{-3} x_9 - 4.21 \times 10^{-2} x_{10} - 2.70 \times 10^{-3} x_{11} + 6.59 \times 10^{-2} x_{12} + 2.59 \times 10^{-2} x_{13} + 3.06 \times 10^{-2} x_{14} - 5.24 \times 10^{-2} x_{15}$
9	$1.85 \times 10^{-4} - 1.12 \times 10^{-3} x_1 + 8.45 \times 10^{-3} x_2 + 6.73 \times 10^{-2} x_3 - 1.43 \times 10^{-4} x_4 - 3.34 \times 10^{-2} x_5 - 3.35 \times 10^{-3} x_6 + 2.18 \times 10^{-2} x_7 - 6.23 \times 10^{-3} x_8 - 2.46 \times 10^{-2} x_9 + 1.36 \times 10^{-2} x_{10} - 2.80 \times 10^{-3} x_{11} + 6.52 \times 10^{-3} x_{12} - 3.59 \times 10^{-2} x_{13} + 1.21 \times 10^{-2} x_{14} - 1.08 \times 10^{-1} x_{15}$
11	$1.27 \times 10^{-4} - 2.76 \times 10^{-3} x_1 - 2.73 \times 10^{-3} x_2 - 1.22 \times 10^{-2} x_3 - 2.85 \times 10^{-4} x_4 + 4.62 \times 10^{-2} x_5 - 1.06 \times 10^{-3} x_6 - 2.13 \times 10^{-3} x_7 - 9.06 \times 10^{-3} x_8 - 2.45 \times 10^{-3} x_9 - 1.12 \times 10^{-3} x_{10} - 2.52 \times 10^{-3} x_{11} - 1.54 \times 10^{-2} x_{12} + 2.54 \times 10^{-2} x_{13} - 4.69 \times 10^{-3} x_{14} - 1.96 \times 10^{-2} x_{15}$
15	$1.85 \times 10^{-4} - 1.27 \times 10^{-3} x_1 - 1.34 \times 10^{-3} x_2 - 1.79 \times 10^{-2} x_3 - 2.49 \times 10^{-4} x_4 - 7.45 \times 10^{-3} x_5 - 6.78 \times 10^{-4} x_6 - 1.20 \times 10^{-3} x_7 - 1.23 \times 10^{-2} x_8 - 1.51 \times 10^{-3} x_9 + 1.67 \times 10^{-2} x_{10} - 2.71 \times 10^{-3} x_{11} - 4.50 \times 10^{-2} x_{12} + 2.42 \times 10^{-2} x_{13} - 3.47 \times 10^{-3} x_{14} + 3.71 \times 10^{-2} x_{15}$

Table 21: RoadRunner DQN: interpretable policy boundary for logistic regression